# Journal of Materials Chemistry A



## **REVIEW**

View Article Online
View Journal



Cite this: DOI: 10.1039/d3ta00254c

# Interphases in aqueous rechargeable zinc metal batteries

Rishivandhiga Jayakumar, ab Daniel M. Harrison, Jun Xu, b \*ab Arun Vishnu Suresh Babu, Chao Luo \*cd and Lin Ma \*cd \*ab \*cd \*ab

Despite extensive research efforts in developing aqueous rechargeable zinc metal batteries (RZMBs) as high-energy-density alternatives to both lithium ion and lithium metal batteries, the commercial prospects for RZMBs are still obfuscated by fundamental scientific questions. In particular, the electrode–electrolyte interphase properties and behaviors are still intensely debated topics in this field. In this review, we provide a comprehensive and thorough overview of the solid electrolyte interphase (SEI) and cathode electrolyte interphase (CEI) in aqueous RZMBs, with an emphasis on the formation mechanisms and characteristics of the SEI and CEI. We then summarize state-of-the-art techniques for characterizing the SEI/CEI to reveal the intrinsic correlation between the functionalities of the interphases and the electrochemical performances. Finally, future directions are proposed, including studies on aqueous SEI/CEI evolution as a function of pH and temperature, as well as SEI/CEI studies for high-energy-density and long-lifetime RZMBs.

Received 13th January 2023 Accepted 11th March 2023

DOI: 10.1039/d3ta00254c

rsc.li/materials-a

## 1. Introduction

To integrate intermittent renewable energy sources and achieve a zero-carbon transition, lithium-ion batteries (LIBs) have been

<sup>a</sup>Department of Mechanical Engineering and Engineering Science, The University of North Carolina at Charlotte, Charlotte, NC 28223, USA. E-mail: jun.xu@uncc.edu; l.ma@uncc.edu

battery Complexity, Autonomous Vehicle and Electrification (BATT CAVE) Research Center, The University of North Carolina at Charlotte, Charlotte, NC 28223, USA Department of Chemistry & Biochemistry, George Mason University, Fairfax, VA 22030. USA. E-mail: cluo@emu.edu

<sup>d</sup>Quantum Science & Engineering Center, George Mason University, Fairfax, VA, 22030, USA predominantly deployed for electric vehicles (EVs) and gridscale battery storage. However, the rapidly growing demand for LIBs has necessitated the development of complementary battery technologies to relieve potential resource crises (*e.g.* lithium, cobalt, nickel).<sup>1</sup>

Rechargeable zinc metal batteries (RZMBs), which were first explored as Cu/Zn piles by Alessandro Volta in 1799,² have regained substantial research interest due to the unique advantages of the zinc metal anode: $^{3,4}$  natural compatibility with aqueous electrolytes, high volumetric capacity (5854 A h L $^{-1}$ ), and higher abundance in the Earth's crust compared with lithium. A variety of cathode materials with earth abundant elements have also been achieved for RZMBs, including diverse



Rishivandhiga Jayakumar is currently a PhD candidate under the guidance of Prof. Lin Ma in the Department of Mechanical Engineering and Engineering Science at the University of North Carolina at Charlotte. She obtained her B. Tech in chemical and electrochemical engineering from CSIR-Central Electrochemical Research Institute (CECRI), India, in 2022. Her research focuses on energy

storage applications, especially developing efficient electrolyte additives for sodium-ion batteries.



Daniel Harrison earned a B.S. in Psychology from George Mason University. He is currently a PhD student in the Department of Chemistry and Biochemistry at George Mason University. His research interests focus on the design and synthesis of novel organic compounds and polymers for sustainable battery technology.

metal oxides (*e.g.* MnO<sub>2</sub>, <sup>5,6</sup> Zn<sub>0.25</sub>V<sub>2</sub>O<sub>5</sub>·nH<sub>2</sub>O, <sup>7</sup> V<sub>2</sub>O<sub>5</sub>, <sup>8,9</sup> Na<sub>2</sub>V<sub>6</sub>-O<sub>16</sub>·1.63H<sub>2</sub>O, <sup>10,11</sup> *etc.*), layered sulfides (*e.g.* TiS<sub>2</sub> (ref. 12)), Prussian blue analogs (*e.g.* zinc hexacyanoferrate<sup>13,14</sup>), and organic materials. <sup>15,16</sup> However, the commercialization of RZMBs with high energy density and long lifetime is still hindered by a few challenges, including zinc dendrite formation/growth, inferior coulombic efficiency (CE), hydrogen or oxygen evolution, and severe electrolyte consumption. <sup>3,4</sup>

Based on the recent advances of RZMBs, it has become clear that most challenges are ascribed to the interphases between electrodes and electrolytes, which have not been thoroughly investigated for RZMBs. Such interphases, known as a solid electrolyte interphase (SEI) on the zinc metal anode surface and a cathode electrolyte interphase (CEI) on the cathode surface, are formed by a combination of electrochemical and chemical reactions at electrode surfaces. The stability of the SEI/CEI will determine the reactions between electrodes and electrolytes, thus affecting cell performance.

## 1.1 History of zinc battery technology

Fig. 1 summarizes the key developments in zinc battery technology over the past two centuries that support our current understanding of the functionality and composition of electrode-electrolyte interphases in RZMBs. The first zinc metal battery, introduced by Alessandro Volta, was demonstrated as zinc metal paired with copper plates in a brine electrolyte in 1799.2 In 1866, Georges Leclanche invented the Leclanche cell, which is a demonstration of early zinc-manganese (Zn-MnO<sub>2</sub>) batteries.4 In 1886, Carl Gassner developed a zinc-carbon battery with a carbon rod as the cathode current collector, while keeping Zn and MnO<sub>2</sub> as the anode and cathode, respectively.<sup>17</sup> A mild acidic aqueous paste containing ammonium chloride (NH<sub>4</sub>Cl) salt with/without zinc chloride (ZnCl<sub>2</sub>) was used as the electrolyte. In 1901, T. Edison invented a rechargeable zincnickel (Zn-Ni) battery system, which was an important starting point for the RZMB technology.18 Unfortunately, these early Zn-Ni batteries with limited cycle life were not of much interest.



Dr Jun Xu received his PhD in Environmental Engineering/ Engineering Mechanics from Columbia University in 2014. He is an Associate Professor at the Department of Mechanical Engineering and Engineering Science at the University of North Carolina at Charlotte (UNC Charlotte). He leads the Vehicle Energy & Safety Research group working on fundamental applied and

research on multiphysics behaviors of battery safety and durability issues and advanced material and structure designs for impact protection.



Dr Chao Luo is an Assistant Professor at the George Mason University. He received his Bachelor's degree from Wuhan University in 2008. Then, he entered the Technical Institute of Chemistry and Physics, Chinese Academy of Sciences and received his Master's degree in 2011. After that, he obtained his PhD degree at the University of Maryland, College Park in 2015 and worked as a postdoc at

the University of Maryland, College Park from 2016 to 2019. His research interests focus on developing new materials and new chemistries for high-performance and sustainable energy storage devices.



Dr Suresh Babu received his PhD in Aerospace Engineering in 2019 from North Carolina State University. He is a teaching assistant professor in the Department of Mechanical Engineering and Engineering Science at the University of North Carolina at Charlotte. His research focuses on renewable energy, fluid dynamics, and nonlinear dynamics.



Dr Lin Ma is an assistant professor in the Department of Mechanical Engineering at UNC Charlotte, USA. He earned his PhD in 2019 at Dalhousie University with a Killam Fellowship. He became a Dr Brad. E. Forch Distinguished Postdoc Fellow (2019–2022) in the U.S. Army Research Laboratory and University of Maryland. Lin's research interests focus on the use of electrochemical and

materials engineering in clean energy technologies (mainly energy storage systems) to address energy and environmental challenges. He is the winner of the 2017 Battery Division Student Research Award and 2021 Battery Division Postdoctoral Associate Research Award given by the Electrochemical Society.

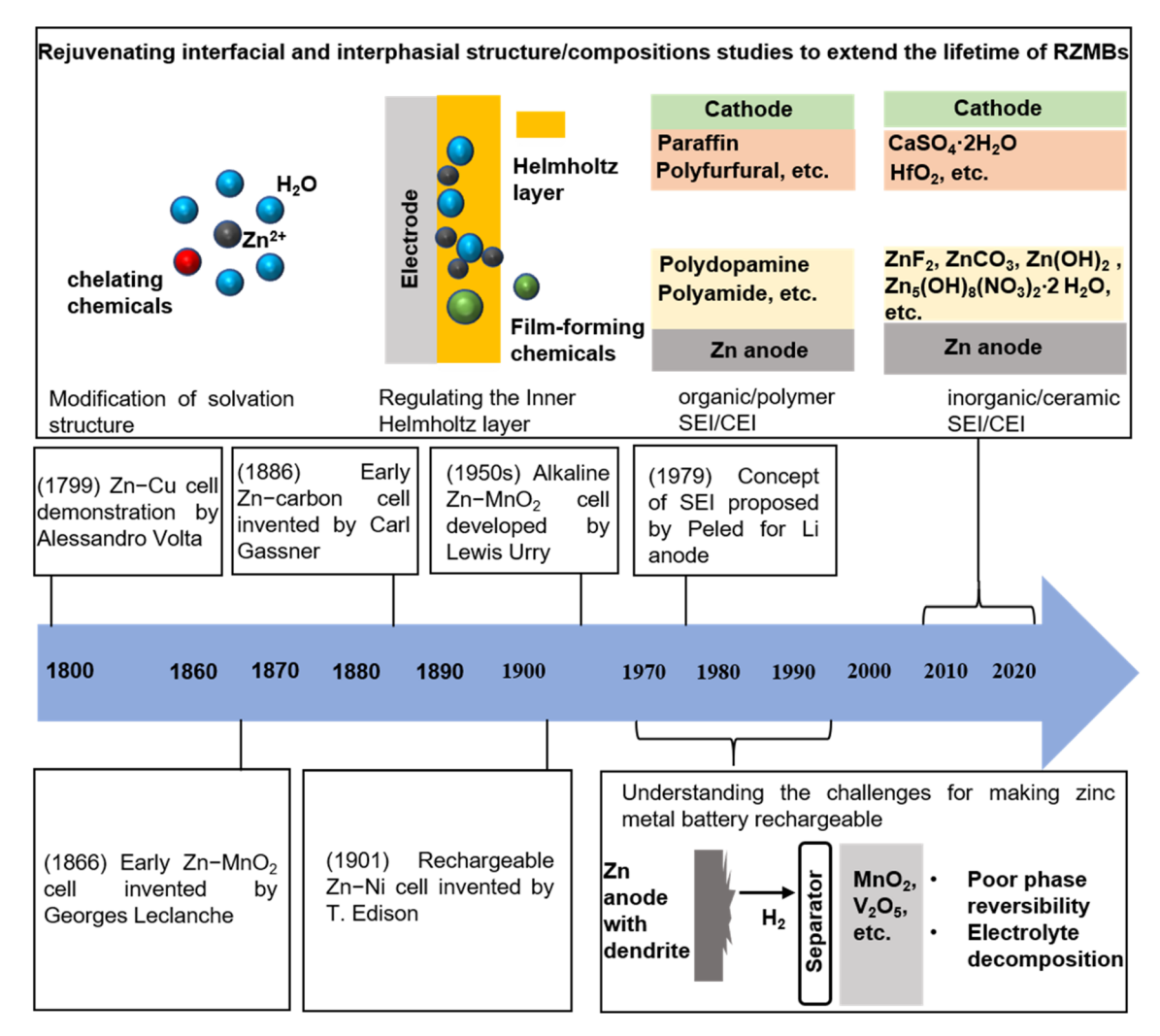


Fig. 1 A summary of the development of Zn metal battery technology.

Additionally, Lewis Urry's development of an alkaline electrolyte in the 1950s made Zn–MnO<sub>2</sub> batteries the dominant technology in the primary battery market, due to improved calendar lifetime and energy density.<sup>19</sup>

Electrode–electrolyte interfacial behaviors drew little attention until the resurgence of efforts to make zinc metal batteries rechargeable between the 1970s and 1990s. Much research has been reported to fundamentally understand the complicated chemistries and materials involved in the mechanism of RZMB failure. In regards to the zinc metal anode, the repeated dissolution/deposition of zinc metal during cell cycling leads to morphological changes and dendrite formation/growth, even with the formation of a ZnO passivation layer in alkaline electrolytes.  $^{20-22}$  Cell capacity fading was also attributed to the cathode, with an example of Mn dissolution from a MnO $_2$  cathode.  $^{5,6,23}$  Additionally, the formation of a CEI consisting of ZnSO $_4\cdot3$ Zn(OH) $_2\cdot n$ H $_2$ O was detected on the MnO $_2$  cathode surface within the aqueous ZnSO $_4$  electrolyte.  $^6$ 

Recently, scientific research on RZMBs has been gaining renewed momentum by leveraging novel materials engineering

in both electrodes and electrolytes with the in-depth understanding of the electrode-electrolyte interfacial behaviors. By transplanting the concepts of the SEI proposed by Peled for the lithium metal anode, <sup>24,25</sup> different approaches (Fig. 1) including Zn<sup>2+</sup> cation solvation structure modification, <sup>26-28</sup> inner Helmholtz layer regulation, <sup>29-31</sup> organic/polymer coating, <sup>32-35</sup> and inorganic/ceramic coating <sup>11,36-39</sup> have been proposed to tune SEI compositions on the zinc metal anode surface with improved mechanical and ionic transport properties to suppress dendrite propagation and hydrogen evolution. Similar strategies have also been applied in tuning the CEI to extend the lifetime of RZMBs. <sup>40-44</sup>

## 1.2 SEI and CEI in RZMBs

The SEI and CEI, composed of insoluble products from reactions between electrodes and electrolytes, are ionic conductors and electronic insulators that prevent continuous side reactions between the electrodes and electrolytes. They have been recognized as key components for the successful implementation of monovalent ion based rechargeable batteries (*e.g.* LIBs,

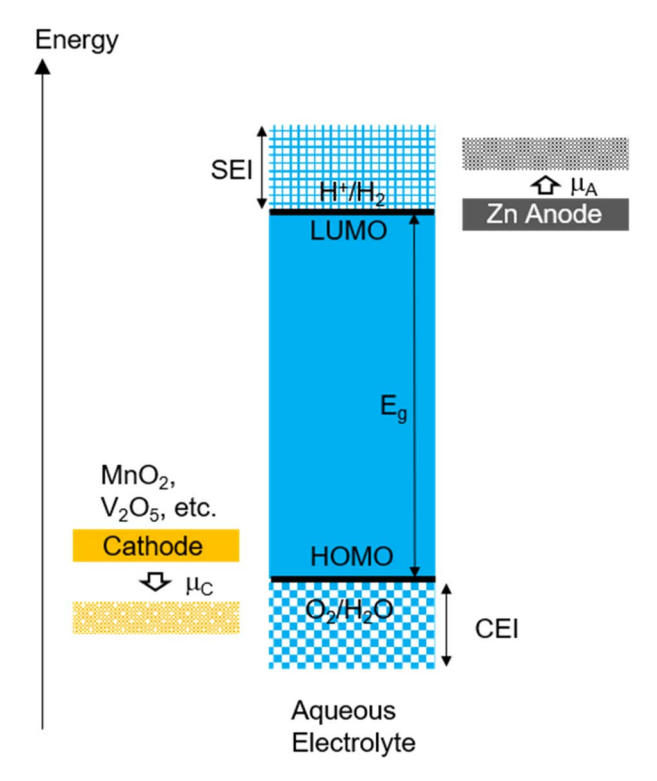


Fig. 2 SEI/CEI formation under electrochemical reduction/oxidation conditions

sodium-ion batteries (SIBs)). According to Goodenough's classical relative electron energy model<sup>45</sup> (Fig. 2), the lowest unoccupied molecular orbital (LUMO) of the electrolyte needs to be higher than the Fermi level of the anode ( $\mu_{\rm A}$ ), while the highest occupied molecular orbital (HOMO) of the electrolyte needs to be lower than the Fermi level of the cathode ( $\mu_{\rm C}$ ) to achieve thermodynamically stable interphases. However, the electrode potential is generally beyond the electrochemical window of electrolytes unless passivation layers (*i.e.* SEI/CEI) block electron transfer between the LUMO or HOMO of the electrolyte and the electrode.

Due to the narrow electrochemical window of water, redox reactions in aqueous electrolytes are limited, and the formation of an SEI/CEI was not considered for aqueous RZMBs until the recent renewed interest in this area. 3,26,31,36,46 To prevent water splitting and improve zinc metal anode reversibility, substantial materials engineering efforts have been made to form and modify the SEI/CEI in RZMBs. The characterization of these SEIs/CEIs has been focused on the morphology, chemical composition, and structure at certain cycling stages. 26,31,36,46 In fact, the functionalities of the SEI/CEI are important links between their properties (morphology, ionic conductivity, solubility, *etc.*) and battery performance. A fundamental understanding of such a correlation would be significant to further reshape the SEI/CEI for better electrochemical performance at the device level.

There are many excellent literature reports discussing Zn electrode–electrolyte interphases in this field. 41,47–49 To differentiate from these reported results, the scope of this review

covers (i) the formation mechanisms of the SEI/CEI, (ii) properties of the SEI/CEI, and (iii) characterization of the SEI/CEI with state-of-the-art techniques. In addition to traditional electrochemical reaction pathways, chemical reaction pathways that largely impact the formation of the SEI/CEI are also discussed. Moreover, theoretical modeling of these reaction pathways and the different interphasial properties of the SEI/CEI are discussed. We focus on the existing knowledge of ionic conductivity, mechanical properties, thermal stability, and chemical and electrochemical stability. To identify the SEI/CEI functions, several important characterization techniques are introduced and discussed with detailed examples. Finally, a perspective on the challenges for understanding and modifying the SEI/CEI in RZMBs is provided, integrating all aspects of the electrode materials, electrolyte materials, and characterization techniques. Currently, the aqueous RZMB field is generating a myriad of exciting research, and this review is not a comprehensive coverage of the topic, but instead, a reflection of the authors' perspectives on current research progress in the realm of the aqueous SEI/CEI.

# 2. Formation of SEI/CEI in aqueous RZMBs

It has been well known that the formation of an SEI/CEI results from the sacrificial decomposition of electrolyte components and RZMBs show no exception. Generally, all the electrolyte components including co-solvents, salts, and electrolyte additives could decompose to form an SEI/CEI. In addition to the electrochemical redox pathway, chemical reaction and artificial fabrication are also realized as complementary SEI/CEI formation routes in aqueous RZMBs. In this section, we will discuss SEI/CEI formation mechanisms through these different routes. The corresponding SEI/CEI chemical compositions and morphology will also be discussed.

## 2.1 SEI formation

Electrons in the zinc anode transfer to the electrolyte components (solvents, salts, or electrolyte additives) when the  $\mu_A$  of the zinc anode is higher than the LUMO of these components, resulting in an electrochemical reduction reaction of electrolyte and formation of an SEI on the zinc metal anode. Typically, such an SEI passivation occurs on metallic zinc at a negative potential of -0.76 V  $\nu s$ . standard hydrogen electrode (SHE), which is much higher than that of lithium metal  $(-3.0 \text{ V } \nu s$ . SHE) and decreases the choices of components that can be reduced. In recent years, to extend the zinc metal anode reversibility, intensified efforts have focused on its SEI, significantly deepening our understanding of this elusive component.

**2.1.1 SEI formation from solvents.** Solvents provide an indispensable medium for ion transport between electrodes in an RZMB. As the main solvent component in aqueous electrolytes, water itself cannot form the SEI due to the gaseous decomposition products (*i.e.* H<sub>2</sub> and O<sub>2</sub>). As a result, continuous parasitic reactions between the zinc anode and electrolytes compromise cell lifetime, while the cell energy density is also

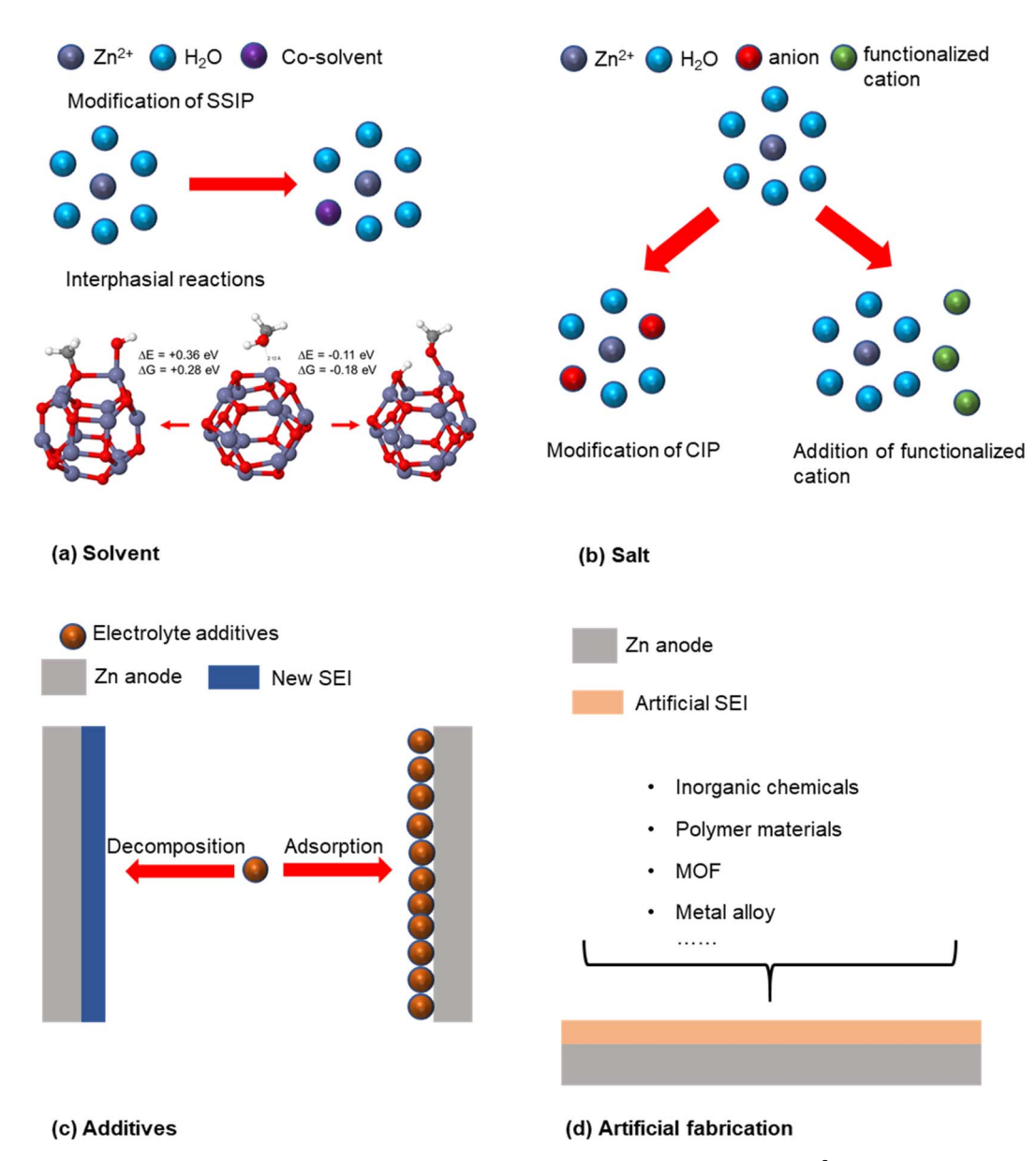


Fig. 3 A summary of the formation pathways of the zinc anode SEI. (a) Co-solvents that modify the  $Zn^{2+}$  cation solvation structure (i.e. SSIP); reproduced from ref. 39, Copyright 2022 the National Academy of Sciences (NAS). (b) Salts that either modify the Zn<sup>2+</sup> cation solvation structure (i.e. CIP) or involve functionalized cations; (c) electrolyte additives that modify interphasial chemistries and interfacial structures by decomposing or adsorbing on the zinc anode surface; (d) artificial SEI composed of various chemicals on the zinc anode surface.

limited by the electrochemical window of water (i.e. 1.23 V). Thanks to the introduction of organic solvents into water as cosolvents for the electrolytes, an SEI has been reported to form on zinc metal anode surfaces with the decomposed products from these organic co-solvents.

The solvation structure, particularly originating from the Zn<sup>2+</sup>-solvent interactions, in a bulk electrolyte with Zn<sup>2+</sup> cationbased salts, have become a topic of importance due to the effect of the Zn<sup>2+</sup>-solvent sheath structure on interfacial structures and SEI chemistries. In a typical aqueous Zn electrolyte, the microstructure is dominated by solvent-separated ion pairs (SSIPs) with few contact ion pairs (CIPs) or aggregate (AGGs) structures occurring.30,31 The typical SSIP is composed of one

Zn<sup>2+</sup> cation surrounded by six water molecules.<sup>50</sup> However, the addition of organic co-solvent molecules with a high Gutmann donor number including methanol (MeOH),51 ethanol (EA),52 ethylene glycol (EG),53-55 acetonitrile (AN),56,57 succinonitrile (SN),58 propylene carbonate (PC),59,60 dimethyl sulfoxide (DMSO),26,61 sulfolane (SL),62 trimethyl phosphate (TMP),63 triethyl phosphate (TEP),64 dimethyl methylphosphonate (DMMP),65 and tetraglyme (G4)66 would modify this SSIP structure by replacing the water in the molecular solvation sheath (Fig. 3a). Multimodal characterizations including Fouriertransform infrared spectroscopy (FTIR), Raman spectroscopy, nuclear magnetic resonance (NMR) spectroscopy and X-ray scattering have been successfully applied to investigate and

Table 1 A summary of co-solvent choices used for improving zinc metal anode reversibility

Solvent chemicals	Ref.	Function	Main SEI components, if any
МеОН	39 and 51	Screen out water and form an SEI	$Zn(OH)_2$ , $Zn(OCH_3)_2$
AN	56 and 57	Screen out water	N/A
SN	58	Screen out water	N/A
DMSO	26 and 61	Screen out water and form an SEI	$Zn_{12}(SO_4)_3Cl_3(OH)_{15} \cdot 5H_2O$ , $ZnSO_3$ , $ZnS$
TEP	64 and 71	Screen out water and form an SEI	$Zn_3(PO_4)_2$ and/or its derivatives, poly- $ZnP_2O_6$
TMP	63 and 72	Screen out water and form an SEI	Zn <sub>3</sub> (PO <sub>4</sub> ) <sub>2</sub> and its derivatives, RZnPO <sub>4</sub> (R represents alkyl groups) aggregation
SL	62	Screen out water	N/A
EG	39 and 53-55	Screen out water and form an SEI	Mainly $Zn(OH)_2$
EA	39 and 52	Form an SEI	$Zn(OH)_2$ , $Zn(OCH_2CH_3)_2$
PC	59 and 60	Screen out water and form an SEI	ZnCO <sub>3</sub>
Fluoromethane or difluoromethane	11	Form an SEI	$\mathrm{ZnF}_2$

elucidate such a solvation structure change, especially when complemented by molecular dynamics (MD) simulations. It is worth noting that the phase field used in MD simulations has to be verified by the experimental results of electrolyte characteristics (e.g. viscosity, density and conductivity).

During the first charging process in an RZMB, the Zn<sup>2+</sup> cation and its solvating molecules will enter the electrical double layer (EDL) of the zinc anode prior to their potential electrochemical reactions. Here, the introduction of co-solvent molecules decreases the number of water molecules in the EDL, thus suppressing the parasitic reactions caused by water splitting. However, the subsequent reaction pathway of co-solvent molecules is still under debate in this field because the reduction potential of some molecules (e.g.  $\sim$  -2.25 V vs. SHE for PC;  $^{67,68} \sim -1.05 \text{ V} \nu s$ . SHE for DMSO<sup>69</sup>) is much lower than that of  $Zn/Zn^{2+}$  (-0.76 V vs. SHE) in spite of direct experimental observation of SEI layers later.26 One possibility is that intimate contact of co-solvent molecules with the zinc metal electrode in the EDL results in a high probability of participating in reduction. Moreover, Borodin et al.70 reported that the actual reduction potential of solvent molecules could change depending on the coordination with cations. In addition to electrochemical reduction, chemical reactions in the interphase can contribute to SEI formation. Ma et al.39 realized the Zn(OH)2 involving SEI formation mechanism through a deprotonation reaction with alcohol family containing co-solvents (Fig. 3a). A summary of co-solvent choices and their functional mechanisms is provided in Table 1.

In summary, developing optimal co-solvents for the purpose of SEI formation is a crucial objective for achieving an RZMB with favorable electrochemical performance. Further understanding the relationship between co-solvent chemistries and SEI chemistries could guide the design and selection of co-solvent molecules. Choosing the optimal co-solvents also requires comprehensive consideration encompassing the ratio to water, flammability, solvation/de-solvation characteristics, and transport properties.

**2.1.2 SEI formation from salts.** Metal salts, significant constituents that dominate the electrolyte pH value, play a pivotal role in determining the electrochemical performance

of RZMBs. They serve as the charge carriers between the cathode and anode and affect the electrolyte's ionic conductivity. Early electrolyte candidates for aqueous RZMBs were based on alkali salts (*e.g.* KOH). Despite a high pH value to suppress the hydrogen evolution reaction (HER), the low Zn<sup>2+</sup> stripping/plating CE and the formation of zinc dendrites with ZnO by-products hinder the development of alkaline electrolytes.<sup>3,73</sup> In contrast, more research efforts have been devoted towards neutral or mildly acidic aqueous electrolytes recently, thus this section will focus on the discussion of salts utilized under these conditions.

A series of salts with  $Zn^{2+}$  as the cation including zinc bis(trifluoromethanesulfonyl)imide  $(Zn(TFSI)_2)$ ,  $^{30,46,74}$  zinc trifluoromethanesulfonate  $(Zn(OTf)_2)$ ,  $^{31,61}$  zinc sulfate  $(ZnSO_4)$ ,  $^{51,75}$  zinc perchlorate  $(Zn(ClO_4)_2)$ ,  $^{76}$  and zinc acetate  $(Zn(Ac)_2)^{77}$  have been investigated in aqueous electrolytes within their very limited solubility (<4 m). There is no significant difference among these different anion chemistries in terms of zinc anode electrochemical performance, except for a better HER suppression in  $Zn(Ac)_2$ -based neutral electrolyte. Among the aforementioned salts, the higher the salt concentration, the better the electrochemical performance obtained. This has been ascribed to the suppression of hydrogen bond networks in the bulk electrolyte without considering any interphasial behavior changes.

To further improve zinc anode reversibility, enlightened by this "water-in-salt" concept, 74,78 substantial efforts have been dedicated to tune the Zn<sup>2+</sup> cation solvation structure (Fig. 3b) and modify the zinc anode SEI by further increasing salt concentration and involving more functionalized cation or anion chemistries. Since zinc chloride (ZnCl<sub>2</sub>) salt can reach a very high concentration of 31 m itself in water at room temperature, its concentration effect on zinc anode reversibility was investigated from 1 m up to 30 m.<sup>79-81</sup> When the concentration of ZnCl<sub>2</sub> is above 5 m, water molecules within the Zn<sup>2+</sup> solvation sheath start to be replaced by Cl<sup>-</sup> and form [ZnCl<sub>4</sub>]<sup>2-</sup>. As a result, the electrolyte electrochemical window stability was improved by decreasing the amount of water in the EDL. Unfortunately, there is no clear report on the change of SEI chemistries here.

Unlike ZnCl2, other zinc salts cannot reach such a high concentration in water. Highly soluble supporting salts with different cation chemistries were introduced to modify electrolyte solvation structures and suppress free water, even in the EDL. For example, to improve zinc anode reversibility in 1 m Zn(TFSI)<sub>2</sub> aqueous electrolyte, Wang et al.<sup>74</sup> introduced another 20 m lithium bis(trifluoromethanesulfonyl)imide (LiTFSI) as a supporting salt. Similarly, 31 m potassium acetate (KAc)82 and 13 m lithium nitrate (LiNO<sub>3</sub>)83 were used as supporting salts with their corresponding zinc salt containing solutions (i.e. 1 m  $Zn(Ac)_2$  and 2.5 m  $Zn(NO_3)_2$ , respectively. To further enrich the SEI chemistries, supporting salts with functionalized cations were also employed instead of simply using these monovalent metal cation-based ones (Fig. 3b). Cao et al.31,46 reported a functionalized cation, trimethyl ethyl ammonium cation (Me<sub>3</sub>EtN<sup>+</sup>), that can be dissolved up to 4 m in water with other 4 m zinc salts. Particularly, the decomposition of the Me<sub>3</sub>EtN<sup>+</sup> cation can generate ethylene, which is the feedstock for the formation of polymeric SEI species. Ma et al.30 reported the effect of different cation ligand chemistries on Zn SEI formation by comparing two supporting salts: tributylmethyl phosphonium-TFSI (P4441-TFSI) and tributyl(2-methoxyethyl)-TFSI  $(P_{444(2O1)}\text{-TFSI}).$ 

In short, the effects of common zinc salts and supporting salts on zinc interphasial behavior are summarized in Table 2. Common zinc salts, except for ZnCl<sub>2</sub>, do not tend to affect electrolyte solvation structure or zinc anode interphasial behavior due to their limited solubility in water (<4 m) at room temperature. Supporting salts, highly soluble in water when dissolved with zinc salts, can be divided into two types: monovalent cation-based and functionalized. The former improve zinc anode reversibility by suppressing the hydrogen bond network in the bulk electrolyte and decreasing the number of water molecules in the EDL. Unfortunately, there are no clear reports on changes in SEI chemistries. The latter supporting salts tend to form an SEI on the zinc anode by decomposing the

cations. More functionalized supporting salt chemistries need to be investigated to further improve zinc anode reversibility.

2.1.3 SEI formation from electrolyte additives. An electrolyte additive is a small amount of a component dissolved in an electrolyte without altering its bulk composition. According to Xu *et al.*, <sup>89</sup> a threshold of 10% is adopted here, below which the new components are considered as electrolyte additives. Unlike the additives in LIBs, the additives in RZMBs are intended to tune interfacial structures by either sacrificing themselves and forming interphases in the initial activation cycles, or by adsorbing on the zinc anode surface to repel water molecules or change the preferred orientation of Zn deposits.

The former sacrificial additives would be consumed and only leave their chemical signatures on the zinc anode surface (Fig. 3c). As a result of the additive's sacrifice, a layer of new chemical species will be formed with a function of conducting  $Zn^{2+}$  cations and blocking electron transfer. This suppresses the parasitic reactions between the zinc metal anode and aqueous electrolytes, thus extending cell lifetime. Zeng *et al.*<sup>32</sup> used dopamine (DA) as an additive in an aqueous electrolyte to form a layer of polydopamine through an electrochemical polymerization process. Alternatively, electrolyte additives can be consumed through chemical reactions and form an SEI layer on the zinc metal anode. Zeng *et al.*<sup>90</sup> reported an SEI layer of  $Zn_3(PO_4)_2 \cdot 4H_2O$  formed by the addition of  $Zn(HPO_4)_2$  as an electrolyte additive. This SEI is formed utilizing the local pH change derived from  $H_2$  evolution.

Compared to the route of additive decomposition, more studies on the development of electrolyte additives have been reported on the route of adsorption. Instead of decomposing and forming a new SEI layer, electrolyte additives in aqueous electrolytes can also adsorb on the surface of the zinc metal anode, dominate the active sites of water splitting, and regulate Zn deposition orientation (Fig. 3c). The functionalized parts of these additives can be cations, anions, or even whole neutral molecules. Zhu *et al.* 91 reported that the tetrabutylammonium

Table 2 A summary of salts used for improving zinc anode reversibility

Classification	Ref.	Salt chemicals	The way of improving zinc anode reversibility	Main SEI components, if any
				· · · · · · · · · · · · · · · · · · ·
Zinc salt	84 and 85	$ZnSO_4$	Manipulate the hydrogen bond network	N/A
	84 and 85	$Zn(OTf)_2$	Manipulate the hydrogen bond network	N/A
	84 and 85	$Zn(TFSI)_2$	Manipulate the hydrogen bond network	N/A
	77	$Zn(Ac)_2$	Affect pH	N/A
	76 and 86	$Zn(ClO_4)_2$	Form an SEI	Cl <sup>-</sup> anion containing species
	79-81	$ZnCl_2$	Screen out water	N/A
Supporting salt	87	LiTFSI	Screen out water	N/A
	83	$LiNO_3$	Screen out water	N/A
	82	KAc	Manipulate the hydrogen bond network	N/A
	88	$LiClO_4$	Manipulate the hydrogen bond network	N/A
	31	Me <sub>3</sub> EtN-OTf	Form an SEI	ZnCO <sub>3</sub> , ZnF <sub>2</sub> , and polymeric species
				(e.g. ZnSO <sub>3</sub> CF <sub>2</sub> CH <sub>2</sub> CH <sub>2</sub> CF <sub>2</sub> SO <sub>3</sub> CF <sub>3</sub> )
	46	Me <sub>3</sub> EtN-TFSI	Form an SEI	ZnCO <sub>3</sub> , ZnF <sub>2</sub> , and polymeric species
		**		(e.g. CH <sub>2</sub> CH <sub>2</sub> CF <sub>2</sub> SO <sub>2</sub> NSO <sub>2</sub> CF <sub>3</sub> )
	30	$P_{444(2O1)}$ -TFSI	Form an SEI	ZnF <sub>2</sub> and polymeric species (e.g.
		(1)		CH <sub>2</sub> CH <sub>2</sub> CF <sub>2</sub> SO <sub>2</sub> NSO <sub>2</sub> CF <sub>3</sub> )

(TBA) cation would electrostatically adsorb and create protective TBA cation layers, which could further restrict the lateral diffusion of  $\mathrm{Zn^{2+}}$  ions and lead to a dendrite-free homogeneous Zn deposition. Ethylene diamine tetraacetic acid tetrasodium salt (Na<sub>4</sub>EDTA) has been reported as a useful additive to suppress H<sub>2</sub> evolution due to the adsorption of the EDTA anion on the zinc anode surface. <sup>92,93</sup> The EDTA anion dominated the active sites for water electrolysis and promoted de-solvation of  $\mathrm{Zn(H_2O)_6}^{2+}$ . Some other electrolyte additive molecules with neutral charge (*e.g.* vanillin, <sup>94</sup> glucose <sup>95</sup>) are also able to improve the zinc metal anode electrochemical reversibility based on a similar adsorption mechanism.

Some selected electrolyte additives used in aqueous Zn electrolytes and their working mechanisms are summarized in Table 3. Typically, electrolyte additives do not affect the Zn<sup>2+</sup> cation solvation structure in the bulk due to their limited amount. The working mechanism of reported electrolyte additives can be classified into two types: 1 modification of interphasial chemistries by decomposing electrolyte additives; 2 alternation of interfacial structures by adsorbing electrolyte additives without any decomposition. Due to the high electrochemical potential of zinc metal (-0.76 V versus the standard hydrogen electrode), most traditional electrolyte additives with a film forming function will not be reduced on the zinc metal anode prior to Zn deposition. This limits the choices of electrolyte additives. As a result, most current studies are focused on developing more electrolyte additives with the function of adsorption instead of decomposition.

**2.1.4 Artificial SEI.** To better tailor the properties of the SEI, researchers have attempted to fabricate an artificial SEI *via* various approaches on the zinc metal anode surface before cell assembly. Typically, the "artificial SEI," with assumed limited solubility in electrolytes, only modifies the surface of a zinc metal electrode without interacting with the other electrode in the cell.

Functioning similarly to an SEI formed *in situ* by the electrolyte components, the main function of an artificial SEI, whether consisting of inorganic chemicals, polymer materials,

metal-organic frameworks (MOF), or metal alloys (Fig. 3d), is to isolate the zinc metal anode from contact with water, and to homogenize Zn deposition. Passerini et al.38 and Zhang et al.104 applied a thin coating with inorganic species (e.g. ZnF<sub>2</sub>,  $Zn_3(PO_4)_2$ - $ZnF_2$ -ZnS) on a zinc metal electrode, and observed improved electrochemical performance of the processed zinc anode in typical aqueous electrolytes, such as higher Zn stripping/plating CE, less hydrogen evolution, and suppressed dendrite growth. Li et al. 105 and Guo et al., 106 on the other hand, coated the surface of a zinc electrode with polymers (e.g. polyacrylamide (PAM)/polyvinylpyrrolidone (PVP), polyvinyl butyand reported remarkable improvements in electrochemical reversibility, especially in dendrite suppression. They attributed this uniform Zn deposition to the guided Zn<sup>2+</sup> migration along polymer chains. The use of MOFs as artificial SEI layer components has also been reported to result in a uniform Zn plating process by creating a zincophilic interface to reduce interfacial charge-transfer resistance and facilitate an electrolyte flux on the zinc anode.34

In addition to these functions discussed above, researchers have also attempted to prepare artificial SEIs with higher ionic conductivity and lower electron conductivity to further suppress side reactions between the zinc metal anode and electrolytes. Yang *et al.*<sup>107</sup> developed a magnesium–aluminum layered double hydroxide (Mg–Al LDH) coating layer as a multifunctional artificial SEI for zinc metal anodes. This artificial SEI layer not only effectively redistributes the Zn<sup>2+</sup> flux near the interphase to prevent dendrite growth, but also dramatically prevents electron tunneling and suppresses parasitic reactions between the zinc anode and electrolyte to extend cell lifetime. A list of selected artificial SEIs and their working mechanisms is summarized in Table 4.

## 2.2 CEI formation

Unlike its counterpart on zinc metal anode surfaces, there has been rather limited effort to understand the CEI in aqueous RZMBs. Few reports were available regarding CEI formation and

Table 3 A summary of electrolyte additives used in aqueous electrolytes for improving zinc anode reversibility

Electrolyte additive chemicals	Ref.	Skeleton aqueous electrolyte and additive amount	Function mechanisms
Dopamine	32	1 M Zn(CF <sub>3</sub> SO <sub>3</sub> ) <sub>2</sub> with 50 mM DA	Form a polymeric species-based SEI
$Zn(H_2PO4)_2$	90	1 M $\text{Zn}(\text{CF}_3\text{SO}_3)_2$ with 25 mM $\text{Zn}(\text{H}_2\text{PO}_4)_2$	Form a $\text{Zn}_3(\text{PO}_4)_2 \cdot 4\text{H}_2\text{O-based SEI}$
LiCl	96	$3 \text{ M ZnSO}_4 + 0.5 \text{ M LiCl}$	Form a Li <sub>2</sub> O/Li <sub>2</sub> CO <sub>3</sub> -based SEI
PEO	97 and 98	1 M ZnSO <sub>4</sub> with 0.5 wt% PEO	PEO adsorbs on the Zn anode surface
Tetrabutylammonium sulfate	91	2 M ZnSO <sub>4</sub> with 0.05 mM TBA <sub>2</sub> SO <sub>4</sub>	TBA <sup>+</sup> cations adsorb on the Zn anode surface
N, N-dimethyl acetamide	99	2 M ZnSO <sub>4</sub> + 10% vol DMA	DMA adsorbs on the Zn anode surface
Na <sub>2</sub> EDTA	92 and 93	1 M ZnSO <sub>4</sub> with 0.075 M Na <sub>2</sub> EDTA	EDTA anions adsorb on the Zn anode surface
$La(NO_3)_3$	100	2 m ZnSO <sub>4</sub> and 0.0085 m La(NO <sub>3</sub> ) <sub>3</sub>	La <sup>3+</sup> adsorbs on the Zn anode surface
Betaine	101	5 m ZnCl <sub>2</sub> + 1 m BT	BT adsorbs on the Zn anode surface
Ammonium acetate	102	2 M ZnSO <sub>4</sub> + 20 mM ammonium acetate	NH <sub>4</sub> <sup>+</sup> (oxygen ligand) and CH <sub>3</sub> COO <sup>-</sup> adsorb on the Zn anode surface
Vanillin	94	2 M ZnSO <sub>4</sub> + 5 mM vanillin	Vanillin adsorbs on the Zn anode surface
Glucose	51	1 M ZnSO <sub>4</sub> + 10 mM glucose	Glucose adsorbs on the Zn anode surface
Benzyltrimethylammonium	103	2 M ZnSO <sub>4</sub> with 0.5 g $\rm L^{-1}$ TMBAC	TMBA <sup>+</sup> adsorbs on the Zn anode surface

coating layer

Artificial SEI chemical components	Ref.	Fabrication method	Function mechanisms
$Zn_3(PO_4)_2$ – $ZnF_2$ – $ZnS$	104	Pre-cycling	Homogenize Zn deposition with a preferred Zn(002) texture
$ZnF_2$	38	Thermal decomposition of a precursor	Suppress dendrite growth
Disordered zinc silicate	108	Directly coating with chemical treatment	Redistribute the Zn <sup>2+</sup> cation flux
Graphitic C <sub>3</sub> N <sub>4</sub> (g-C <sub>3</sub> N <sub>4</sub> ) nanosheets	109	Directly coating with heating treatment	Redistribute the Zn <sup>2+</sup> cation flux through a crystallographic match
Zinc benzene tricarboxylate	110	Blade coating	Regulate both ionic conduction and electric field at the Zn metal anode surface
Cu <sub>3</sub> (BTC) <sub>2</sub> MOF	111	Slurry coating	Confine non-aqueous species inside
PVDF with UiO-66 MOF	34	Slurry coating	Nanowetting effect
Poly(vinyl butyral) (PVB)	106	Spin-coating	Strong adhesion to the Zn surface with hydrophilicity
Polyacrylamide (PAM)/ polyvinylpyrrolidone (PVP) binary blend layer	105	Slurry coating	Guide the migration of Zn <sup>2+</sup> along polymer chains
Magnesium-aluminum layered double hydroxide (Mg-Al LDH)	107	Slurry coating	Redistribute the Zn <sup>2+</sup> cation flux near the interphase

Table 4 A summary of selected artificial SEIs for improving zinc anode reversibility

evolution mechanisms, chemical compositions, and functions. There are at least three reasons for the lack of CEI studies in aqueous RZMBs:

- (1) first, as compared to the more pressing necessity associated with zinc metal anode SEI studies, there has been a lack of motivation to understand the CEI. The irreversible issues from the zinc metal anode, especially dendrite growth, have been regarded to cause prompt cell failure. Without a working Zn stripping/plating process, the cathode materials do not form dendrites that short the cell immediately. Due to the limited choices of cathode materials for RZMBs, more research is focused on developing novel cathode materials with higher specific capacity and higher average voltage, and exploring their relevant Zn storage mechanisms.
- (2) The complicated chemical compositions on cathode surfaces make it difficult to clearly discern the CEI products from chemical reactions or even electrochemical oxidation of electrolyte components. Further complications are introduced by the competition between the Zn<sup>2+</sup> cation and proton insertion on cathode surfaces, and its concomitant reactions with electrolyte components.
- (3) More importantly, the operating potentials of most cathode materials in aqueous RZMBs are close to or higher than that of the oxygen evolution reaction (OER) of water solvent; therefore, the decomposition of electrolyte components might not be mandatory to in situ form a CEI directly.

As a traditional cathode material used in aqueous RZMBs, MnO2 has been widely studied for decades and is used as a common testing vehicle for electrolyte development. Taking the MnO<sub>2</sub> cathode as an example, this section intends to cover a few important advances made regarding the CEI for aqueous RZMBs. More emphasis will be placed on the development of artificial CEI chemistries, whose functions have become

a subject of vital importance for extending the lifetime of aqueous RZMBs.

In many aqueous RZMBs that use MnO2 or other oxide cathode materials, Zn2+ intercalation is accompanied by proton intercalation and concomitant deposition of a layered double hydroxide (LDH) on the cathode surface as a special spontaneous "CEI". 112,113 The formation of LDH comes from the reaction of OH<sup>-</sup>, which remains after H<sup>+</sup> intercalation, with Zn<sup>2+</sup> and the electrolyte anions. 114,115 Zn<sub>4</sub>(OH)<sub>6</sub>SO<sub>4</sub>·xH<sub>2</sub>O is the typical LDH composition when ZnSO<sub>4</sub> is used as the salt in aqueous electrolyte. Although this LDH layer can buffer electrolyte pH to sustain the proton intercalation, it could detach off the cathode and limit cell lifetime during storage resting.116 With emerging identification and acknowledgement of such a special "CEI", more research could be done to further figure out other interfacial behaviors (e.g. Zn2+ cation de-solvation process) on this "CEI".

Most aqueous RZMBs with MnO2 or other oxide cathode materials could exhibit significant capacity fade over long-term cycling due to the dissolution of Mn2+ or other transition metal cations into the electrolyte. 117,118 To address this issue, research efforts on the CEI have been made with respect to both in situ formation and artificial fabrication (Fig. 4). Zhou et al.42 developed an in situ electrochemically formed CaSO<sub>4</sub>·2H<sub>2</sub>O CEI layer on the surface of a Ca2MnO4 cathode (Fig. 4a). This CEI layer can effectively suppress the Mn2+ dissolution, reduce the activation energy, facilitate Zn2+ intercalation/de-intercalation, and reduce impedance. Zhu et al.119 in situ formed a CEI composed of ZnCO<sub>3</sub> by tuning the Zn<sup>2+</sup> solvation structure with urea to form a [Zn(H<sub>2</sub>O)<sub>2</sub>(urea)<sub>3</sub>]<sup>2+</sup> complex in electrolyte. This CEI successfully inhibits the Mn dissolution from the Na<sub>0.1</sub>MnO<sub>2</sub>-·0.5H<sub>2</sub>O cathode, contributing to cathode structure integrity.

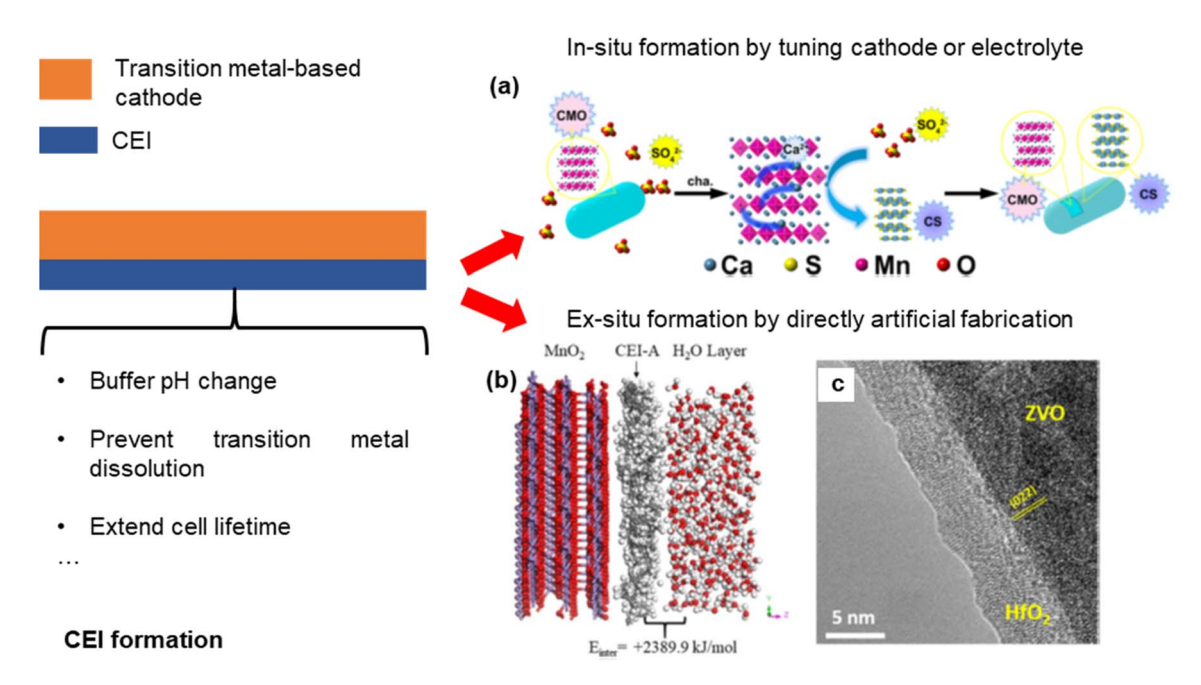


Fig. 4 A summary of the CEI formation pathways in aqueous RZMBs with transition metal-based cathodes. (a) An example of in situ formation of a CaSO<sub>4</sub>·2H<sub>2</sub>O CEI layer by tuning cathode composition, reproduced from ref. 42, Copyright 2019 the American Chemical Society; (b) an example of artificially coating paraffin as a CEI layer on a MnO<sub>2</sub> cathode, 40 reproduced from ref. 40, Copyright 2022 the American Chemical Society; (c) an example of an artificial ALD for coating  $HfO_2$  as a CEI layer on a  $Zn_3V_2O_7(OH)_2 \cdot 2H_2O$  cathode, reproduced from ref. 44, Copyright 2019 the American Chemical Society.

Due to the limited choice in electrolyte components functionalized for CEI formation, more efforts have been concentrated on developing novel artificial CEI chemistries. Chen et al.40 directly coated paraffin on the surface of MnO2 and ZnMn<sub>2</sub>O<sub>4</sub> cathodes as a CEI to suppress Mn<sup>2+</sup> dissolution and prevent contact with water (Fig. 4b). Cell lifetime was dramatically extended even with a very high cathode mass loading, over 20 mg cm<sup>-2</sup>. Such artificial CEI strategies have also been applied in vanadium-based cathode materials to successfully prevent vanadium dissolution and improve cell lifetime. Alshareef et al.44 reported an ultrathin hafnium(IV) oxide (HfO2) film as a CEI on the surface of Zn<sub>3</sub>V<sub>2</sub>O<sub>7</sub>(OH)<sub>2</sub>·2H<sub>2</sub>O that is

uniformly deposited by atomic layer deposition (ALD, Fig. 4c). Miao et al.120 introduced a CEI with a SrCO3 coating layer by incorporating Sr<sup>2+</sup> ions into V<sub>2</sub>O<sub>5</sub> layers as a sacrificial additive. Chen et al. 121 constructed a CEI on the surface of a V<sub>2</sub>O<sub>5</sub> cathode via a polymerization process of heterocyclic aromatic chains and benzene derivatives (e.g. pyrrole, aniline, thiophene). Selected recent studies on aqueous CEIs are summarized in Table 5.

Redox-active organic materials and polymers have also been considered attractive cathodes of RZMBs due to their low cost, abundance, high sustainability, environmental benignity, and great structural tunability. Although various organic cathode

Table 5 A summary of selected CEIs for preventing transition metal dissolution and extending cell lifetime

CEI components	Ref.	Fabrication method and cathode material	Function mechanisms
CaSO <sub>4</sub> ·2H <sub>2</sub> O	42	In situ electrochemically formed on the surface of $Ca_2MnO_4$	Suppress the Mn <sup>2+</sup> dissolution and facilitate Zn <sup>2+</sup> transportation
ZnCO <sub>3</sub>	119	In situ formed on the surface of a Na <sub>0.1</sub> MnO <sub>2</sub> ·0.5H <sub>2</sub> O cathode by tuning the solvation structure	Inhibit the Mn <sup>2+</sup> dissolution
Paraffin	40	Artificially coated on the surface of a MnO <sub>2</sub> and ZnMn <sub>2</sub> O <sub>4</sub> cathode	Suppress Mn <sup>2+</sup> dissolution and prevent water decomposition
Hafnium(IV) oxide (HfO <sub>2</sub> )	44	Deposited on the surface of a $Zn_3V_2O_7(OH)_2 \cdot 2H_2O$ cathode by ALD	Prevent vanadium dissolution
SrCO <sub>3</sub>	120	Artificially introducing Sr <sup>2+</sup> ions into V <sub>2</sub> O <sub>5</sub> layers	Prevent vanadium dissolution
Conductive heterocyclic aromatic chains	121	Artificially polymerizing benzene derivatives on the surface of V <sub>2</sub> O <sub>5</sub>	Prevent vanadium dissolution and buffer the $V_2O_5$ volume change

materials have been developed with different redox mechanisms for RZMBs, their performances, in terms of specific capacity and voltages, have not been comparable with V-based and Mn-based inorganic compounds so far. 15,122 Moreover, severe capacity decay was observed owing to the dissolution of small organic compounds into the electrolytes. Polymerizing organic compounds to form high-molecular-weight polymers is an effective strategy for addressing the high solubility challenge, but a large amount of carbon additives is required to increase the cathode electronic conductivity, sacrificing the battery energy density. In the authors' opinion, more efforts should be devoted to rational design of organic cathode materials with high capacity, long cycle life, high cycling stability, and fast charging capability in RZMBs prior to detailed CEI

#### Properties of SEI/CEI 3.

An ideal SEI or CEI is considered to be highly ionically conductive, electronically insulative, thermally stable at elevated temperatures, chemically stable against electrode materials, and capable of suppressing side reactions between electrodes and electrolytes even under the significantly high mechanical pressure caused by morphology change. It is well known that the structure, morphology, and chemical composition of the SEI/CEI determine the properties of the SEI/CEI. In this section, the properties of the SEI/CEI, including ionic conductivity, mechanical strength, thermal stability, and chemical stability will be comprehensively reviewed and discussed.

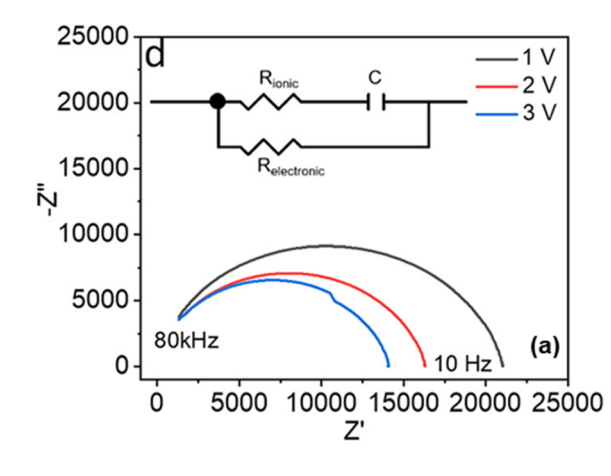
## 3.1 Zn<sup>2+</sup> ion transport properties of SEI/CEI

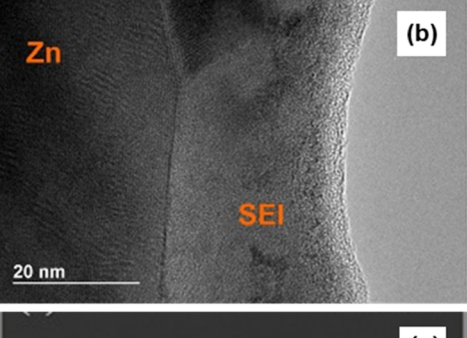
The Zn<sup>2+</sup> ionic conductivities of the SEI or CEI are closely related to the components of the SEI or CEI, and the Zn<sup>2+</sup> migration mechanism within the SEI or CEI. Due to the thin thickness (even at the nanometer scale), complex chemical composition, and inhomogeneous nature, direct experimental methods to determine the SEI or CEI ionic conductivity are challenging to establish. The detailed Zn2+ transportation mechanism through the SEI/CEI has not been elucidated. As a result, indirect experimental results combined with theoretical calculations were widely used to make an estimation on the Zn2+ ionic conductivity of the SEI or CEI and establish the Zn2+ transportation mechanism through the SEI or CEI. In this part, the Zn<sup>2+</sup> ionic conductivities of several typical single SEI or CEI components are discussed.

3.1.1 ZnF<sub>2</sub>. ZnF<sub>2</sub> is the major product in F-containing aqueous electrolytes and the main choice of an artificial SEI/CEI component. Leveraging electrochemical impedance spectroscopy (EIS) testing, equivalent circuit fitting (Fig. 5a), and the nudged elastic band (NEB) calculations, Passerini et al.38 obtained the ionic conductivity value of ZnF<sub>2</sub> at around 10<sup>-4</sup> mS cm<sup>-1</sup> at room temperature, which is 5 orders of magnitude lower than that reported by Zhi et al.37 Apparently, the Zn2+ conductivity through a ZnF2 containing SEI/CEI needs to be further explored.

3.1.2 ZnS. ZnS is a typical SEI/CEI component which contributes to cell performance improvement. Guo et al. 123 investigated the ionic conductivity of the ZnS film alone with a result of  $1.3 \times 10^{-5} \text{ S cm}^{-1}$ , which enables  $\text{Zn}^{2+}$  diffusion through this protective film.

## An elusive ionic conduction process in aqueous Zn SEI





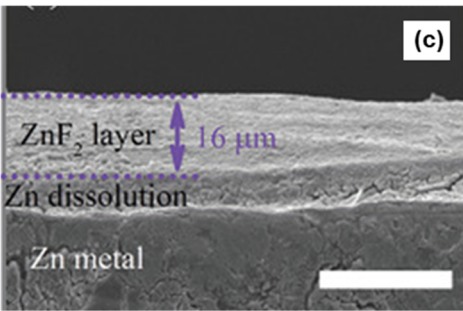


Fig. 5 An example to demonstrate the elusiveness of understanding the Zn<sup>2+</sup> conduction process through the SEI/CEI. (a) An example of an indirect experimental technique (i.e. EIS) for characterizing the ionic conductivity of ZnF<sub>2</sub>, reproduced from ref. 38, Copyright 2019 the American Chemical Society. (b) TEM of the Zn SEI formed with aqueous 4 m Zn(TFSI)<sub>2</sub> + 4 m  $P_{444(2O1)}$ -TFSI after 40 h of cycling (0.5 mA cm<sup>-2</sup>, 0.5 mA h cm<sup>-2</sup> per cycle), reproduced from ref. 30, Copyright 2021 Wiley. (c) Cross-sectional SEM of a Zn SEI with an artificial ZnF<sub>2</sub> layer in aqueous 2 M ZnSO<sub>4</sub> after 50 h of cycling (2 mA cm<sup>-2</sup>,1 mA h cm<sup>-2</sup> per cycle), reproduced from ref. 37, Copyright 2021 Wiley VCH.

- **3.1.3**  $\text{Zn}_3(\text{PO}_4)_2 \cdot 4\text{H}_2\text{O}$ . The ionic conductivity of  $\text{Zn}_3(\text{PO}_4)_2 \cdot 4\text{H}_2\text{O}$  was obtained through EIS at room temperature by Zeng *et al.*<sup>90</sup> A high value of  $7.2 \times 10^{-5}$  S cm<sup>-1</sup> was observed, which is consistent with the claim that  $\text{Zn}_3(\text{PO}_4)_2 \cdot 4\text{H}_2\text{O}$  is a highly  $\text{Zn}^{2+}$  conductive solid electrolyte material.<sup>124</sup>
- **3.1.4**  $Zn_4(OH)_6SO_4 \cdot xH_2O$ .  $Zn_4(OH)_6SO_4 \cdot xH_2O$  is a well-known product generated in the CEI when H<sup>+</sup> insertion occurs at the cathode. <sup>112</sup> Zhu *et al.* <sup>125</sup> realized its high ionic conductivity of 0.26 mS cm<sup>-1</sup> at room temperature using EIS.
- 3.1.5 Zinc silicate. As a novel artificial SEI component, zinc silicate with a disordered structure was reported to achieve a high ionic conductivity of 9.29 mS cm $^{-1}$  at room temperature. The absence of grain boundaries along the  $\rm Zn^{2+}$  transport tunnel could be the reason for the improved  $\rm Zn^{2+}$  ionic conductivity.
- **3.1.6 Gelatin.** Gelatin is one type of polymeric chemical used as an artificial SEI/CEI to prevent side reactions between aqueous electrolytes and electrodes. A high ionic conductivity of  $3.6 \times 10^{-2} \ \mathrm{S \ cm^{-1}}$  was reported by Choi *et al.* <sup>126</sup> using EIS.

The actual  $Zn^{2^+}$  ionic conductivity of the SEI or CEI is not only determined by each single component, but also by the way these species are combined. Unlike the SEI of Li metal anodes, there is no mature model to describe the SEI or CEI structures of aqueous RZMBs. Notably, the reported Zn SEI thickness is highly inconsistent and tends to cover a wide range, from  $\sim\!20$  nm even up to  $16~\mu m^{30,37}$  (Fig. 5b and c), which is in conflict with the classical theory of SEI thickness on non-aqueous Li-based batteries  $^{127,128}$  ( $\sim\!30$  nm). The traditional "ion hopping" mechanism within the crystalline lattice may not be able to fully explain the  $Zn^{2^+}$  ionic conduction across such a thick SEI/CEI. To date, few efforts have been devoted to understanding the detailed  $Zn^{2^+}$  conduction mechanism. In addition, direct experimental evaluation of SEI/CEI conductivity should also be developed in the future.

## 3.2 Mechanical properties of SEI/CEI

Typically, SEI mechanical stress will be caused by significant morphological changes of the zinc metal underneath the SEI during the Zn stripping/plating process. When such a stress is beyond the stress limit of the SEI, the zinc metal anode could suffer from SEI fracture, re-exposure to the electrolyte with more side reactions, and even Zn dendrite growth (Fig. 6a). Consequently, the mechanical properties (e.g. Young's modulus, shear modulus) of the SEI are critical for extending the zinc metal anode lifetime.

Substantial efforts have been devoted to characterizing the Young's modulus of the Zn SEI using atomic force microscopy (AFM)<sup>130</sup> and correlating it with the dendrite growth process. Zhang *et al.*<sup>131</sup> successfully suppressed Zn dendrite growth by coating a graphite SEI on the Zn surface and ascribed the results to the lower Young's modulus of graphite with good ductility and compressibility. Zhang *et al.*<sup>132</sup> reported that agarose gel was able to suppress Zn dendrite formation due to its high Young's modulus. It is counterintuitive to see such different claims dependent on Young's modulus. This could result from complicated mechanisms of dendrite formation/growth,

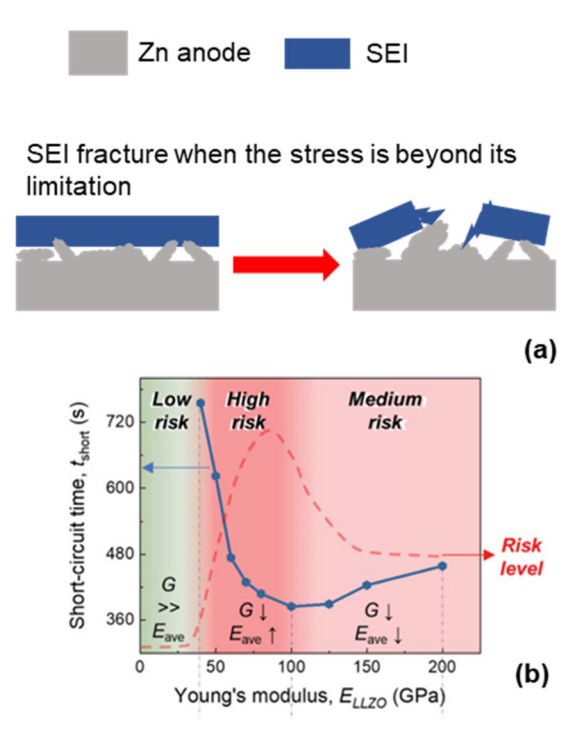


Fig. 6 The effect of interphasial mechanical properties on dendrite formation/growth. (a) A schematic showing the process of SEI fracture when the stress caused by Zn deposition is beyond its limitation. (b) Cell short-circuit time caused by dendrite growth as a function of Young's modulus of  $\text{Li}_7\text{La}_3\text{Zr}_2\text{O}_{12}(\text{LLZO})$ , reproduced from ref. 129, Copyright 2021 Wiley.

different chemical compositions of the SEI/CEI, and limited understanding of the relationship between Young's modulus change and dendrite growth. Borrowing the knowledge from Li dendrites, Xu *et al.*<sup>129</sup> suggested that the Young's modulus of ceramic solid state electrolytes may not have a linear relationship with dendrite suppression (Fig. 6b).

Additionally, Viswanathan *et al.*<sup>133</sup> highlighted the importance of the shear modulus on suppressing dendrite formation and growth using machine learning. Ma *et al.*<sup>46</sup> experimentally demonstrated the function of ZnCO<sub>3</sub> in suppressing dendrite growth due to the higher shear modulus of ZnCO<sub>3</sub> (49 GPa) compared with Zn (37 GPa). Evaluation of the effect of different mechanical properties on suppressing dendrite growth should also be considered in the future.

## 3.3 Thermal stability of SEI/CEI

Due to the use of water as the major component of electrolytes, aqueous RZMBs will not suffer from fire or explosion triggered by thermal instability of the SEI at elevated temperatures. However, it is also important to achieve an SEI or CEI with better thermal stability for aqueous RZMBs to secure a longer lifetime considering current battery technology is expected to operate across wide temperature ranges. According to Dahn *et al.*, <sup>134,135</sup> the degradation of the SEI/CEI above room temperatures (typically >40 °C) is the main reason for cell lifetime degradation caused by the involvement of more parasitic

reactions. Chen et al. 121 recently extended the lifetime of V<sub>2</sub>O<sub>5</sub>/ Zn cells at 60 °C by artificially polymerizing pyrrole as a thermally stable CEI to prevent V2O5 dissolution. More exploration of the thermal stability of SEIs/CEIs in aqueous RZMBs should also be considered in the future, especially when flammable chemicals (e.g. methanol39,51) are being used as co-solvents in aqueous electrolytes.

### 3.4 Chemical and electrochemical stability of SEI/CEI

To support a longer lifetime in aqueous RZMBs, the SEI/CEI must remain stable in the bulk electrolyte against both chemical reactions and electrochemical degradation. According to Suo et al., 136 an aqueous SEI/CEI faces much more severe challenges (e.g. dissolution) from the perspective of chemical degradation than its nonaqueous counterpart due to the unique properties of water, including a high dielectric constant, large dipole moment, and high acceptance/donor numbers. Ma et al.39 investigated the effect of potential SEI dissolution in water on zinc metal anode reversibility. The use of MeOH as solvent enabled the formation of a Zn(OH)<sub>2</sub> containing SEI on the surface of the zinc metal anode (Fig. 7a and b), which further improved interphasial ionic conductivity and suppressed electronic conductivity.39 However, with the addition of water into the MeOH, the reversibility of the zinc metal anode (Fig. 7c and d) decreased, which could result from the dissolution of the SEI. From this perspective, the alteration of the chemical components and the structures of the SEI/CEI should be investigated to build chemically and electrochemically stable interphases, for example, taking advantage of the most recently developed concept of bilayer interphases which include an inner inorganic-rich layer and outer polymeric layer and demonstrate a superior stability against both the anode and cathode.137

Compared to non-aqueous LIBs, specific studies on the electrochemical stability of the SEI/CEI in aqueous RZMBs are not urgent due to the narrow electrochemical window of water.

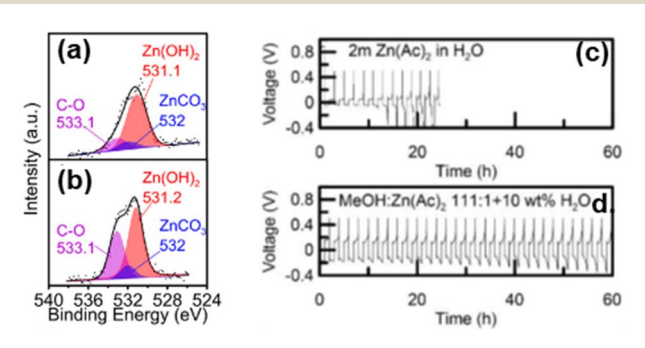


Fig. 7 The effect of water on zinc metal anode reversibility.<sup>39</sup> (a and b) XPS spectra of O 1s for zinc metal anodes corresponding to samples obtained from Zn $|Zn|(100 \mu m)$  symmetric cells at a zero state of charge after (a) 20 h and (b) 200 h of cycling (2.5 mA cm $^{-2}$ , 2.5 mA h cm $^{-2}$  per cycle) with 111:1 (MeOH:Zn(OTf)<sub>2</sub> by mol) electrolyte at room temperature. (c and d) Voltage vs. time for Cu|Zn (10  $\mu$ m) cells cycled with 2.93 mA cm<sup>-2</sup>, 2.93 mA h cm<sup>-2</sup> and 50% Zn utilization per cycle with different water content as labeled in the panel. Reproduced from ref. 39, Copyright 2022 NAS.

- Chemical compositions (XPS, XRD, EDS, etc.)
- Morphology (SEM, TEM, AFM, etc.)

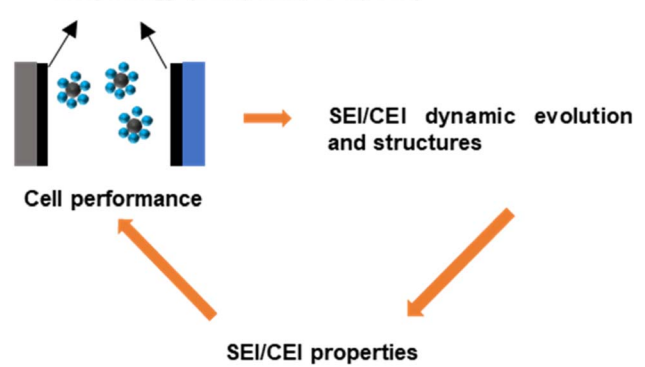


Fig. 8 A schematic of the relationship between SEI/CEI characterization and cell performance improvement.

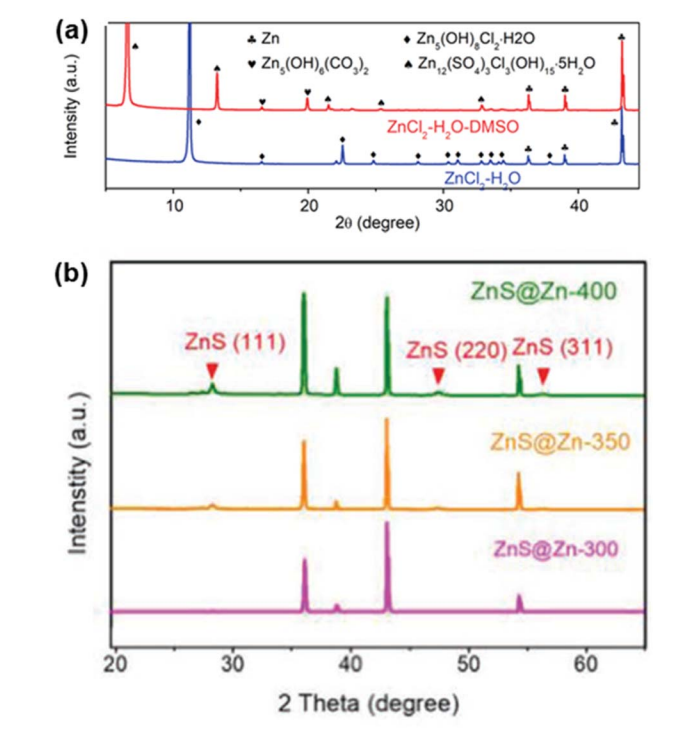


Fig. 9 Characterization of the aqueous Zn SEI using XRD. (a) XRD patterns of Zn anodes after plating/stripping cycles in ZnCl<sub>2</sub>-H<sub>2</sub>O-DMSO and ZnCl<sub>2</sub>-H<sub>2</sub>O electrolytes. Reproduced from ref. 26, Copyright 2020 American Chemical Society. (b) XRD patterns of ZnS@Zn foils at different temperatures. Reproduced from ref. 123, Copyright 2020 Wiley VCH.

Once the electrochemical window of water can be expanded to a competitive level compared to non-aqueous solvents, this topic would be worth considering more in the future.

## Characterization of SEI and CEI

To date, considerable efforts have been devoted to developing artificial SEIs/CEIs and advanced electrolytes for aqueous

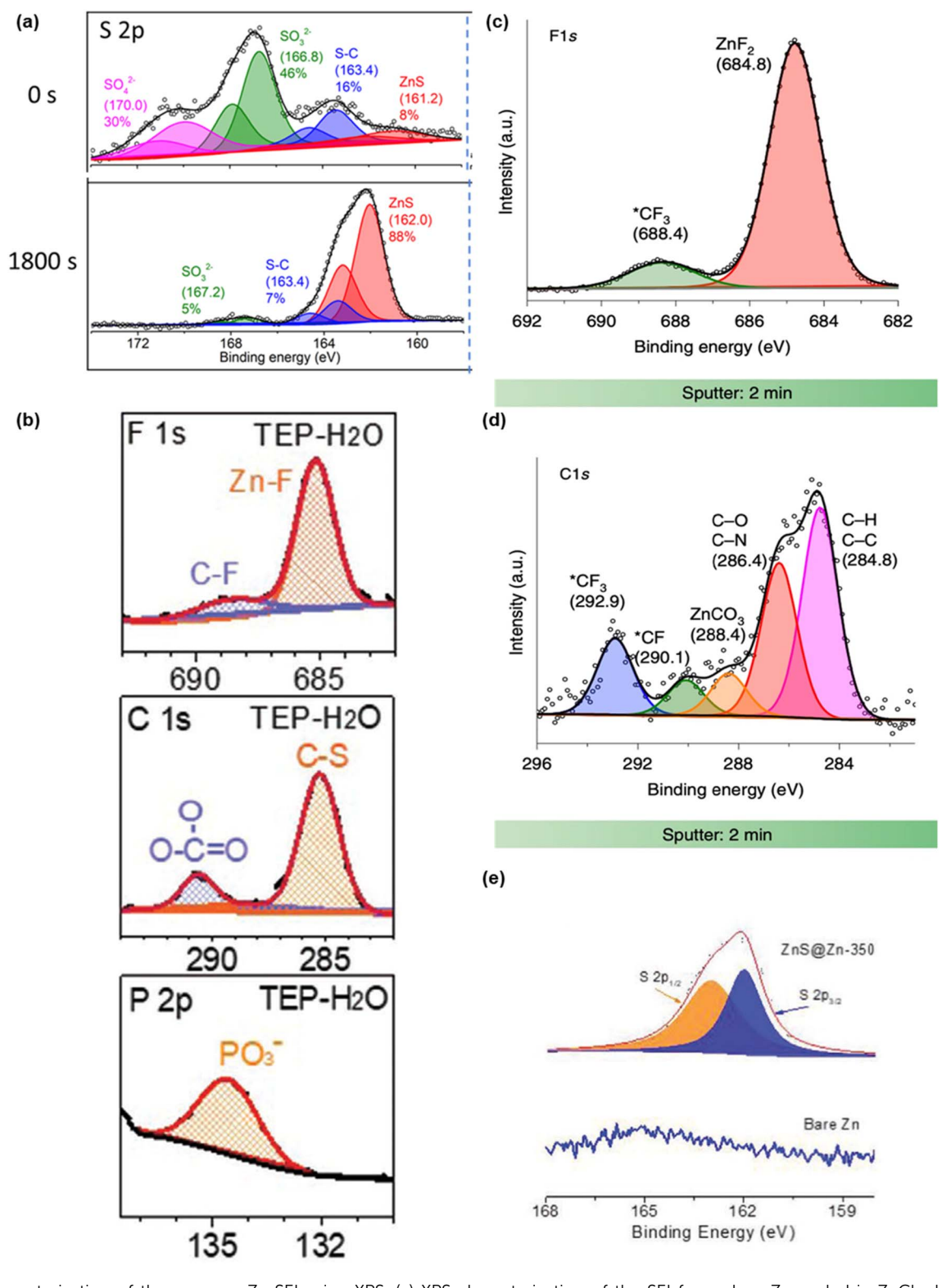


Fig. 10 Characterization of the aqueous Zn SEI using XPS. (a) XPS characterization of the SEI formed on Zn cycled in  $ZnCl_2-H_2O-DMSO$  electrolyte. Reproduced from ref. 26, Copyright 2020 American Chemical Society. (b) XPS spectra of the F 1s, C 1s, and P 2p on the zinc anode after cycling in  $Zn(OTf)_2-TEP-H_2O$  electrolyte. Reproduced from ref. 64, Copyright 2021 Wiley VCH. XPS spectra depth profiles of F 1s (c) generated after  $Ar^+$  sputtering for 2 min, and of C 1s (d) after 2 min on zinc metal cycled in 4 m  $Zn(OTf)_2 + 0.5$  m  $Me_3EtN-OTf$ . Reproduced from ref. 31, Copyright 2021 Springer Nature. (e) XPS spectra of bare Zn and ZnS@Zn foil with S 2p spectra. Reproduced from ref. 123, Copyright 2020 Wiley VCH.

RZMBs. The nano-structured artificial SEI/CEI layers containing CaCO<sub>3</sub>, TiO<sub>2</sub>, polyamide, polyimide, metal organic frameworks, etc. have been employed to coat on the surface of the zinc metal anode or cathode and stabilize both electrodes for dendrite-free and high-performance aqueous RZMBs. In addition, advanced aqueous electrolytes that can in situ form SEIs/CEIs containing ZnF<sub>2</sub>, ZnCO<sub>3</sub>, ZnS, ZnSO<sub>3</sub>, ZnSO<sub>4</sub>, Zn<sub>3</sub>(PO<sub>4</sub>)<sub>2</sub>, etc. have been identified. This section discusses the state-of-the-art techniques that have been widely used to characterize the SEI/CEI layer mainly from the perspective of morphology and chemical compositions, including X-ray photoelectron spectroscopy (XPS), X-ray diffraction (XRD), focused ion beam (FIB) detection, Raman spectroscopy, AFM, scanning electron microscopy (SEM), transmission electron microscopy (TEM), energy dispersive spectroscopy (EDS), and electrochemical quartz

crystal microbalance (EQCM) analysis (Fig. 8). We aim to provide a fundamental understanding toward the state-of-theart SEI/CEI characterization techniques and the properties of the SEI/CEI in aqueous RZMBs. The correlation between the composition and the structure of SEIs/CEIs and their properties will also be discussed.

#### Characterization of SEI

#### 4.1.1 Characterization of SEI chemical compositions

4.1.1.1 XPS and XRD. An SEI is typically composed of complex chemical compositions. It is significant to deconvolute the chemical information using multiple techniques simultaneously to further understand the SEI properties. According to published literature, the most common techniques for the SEI

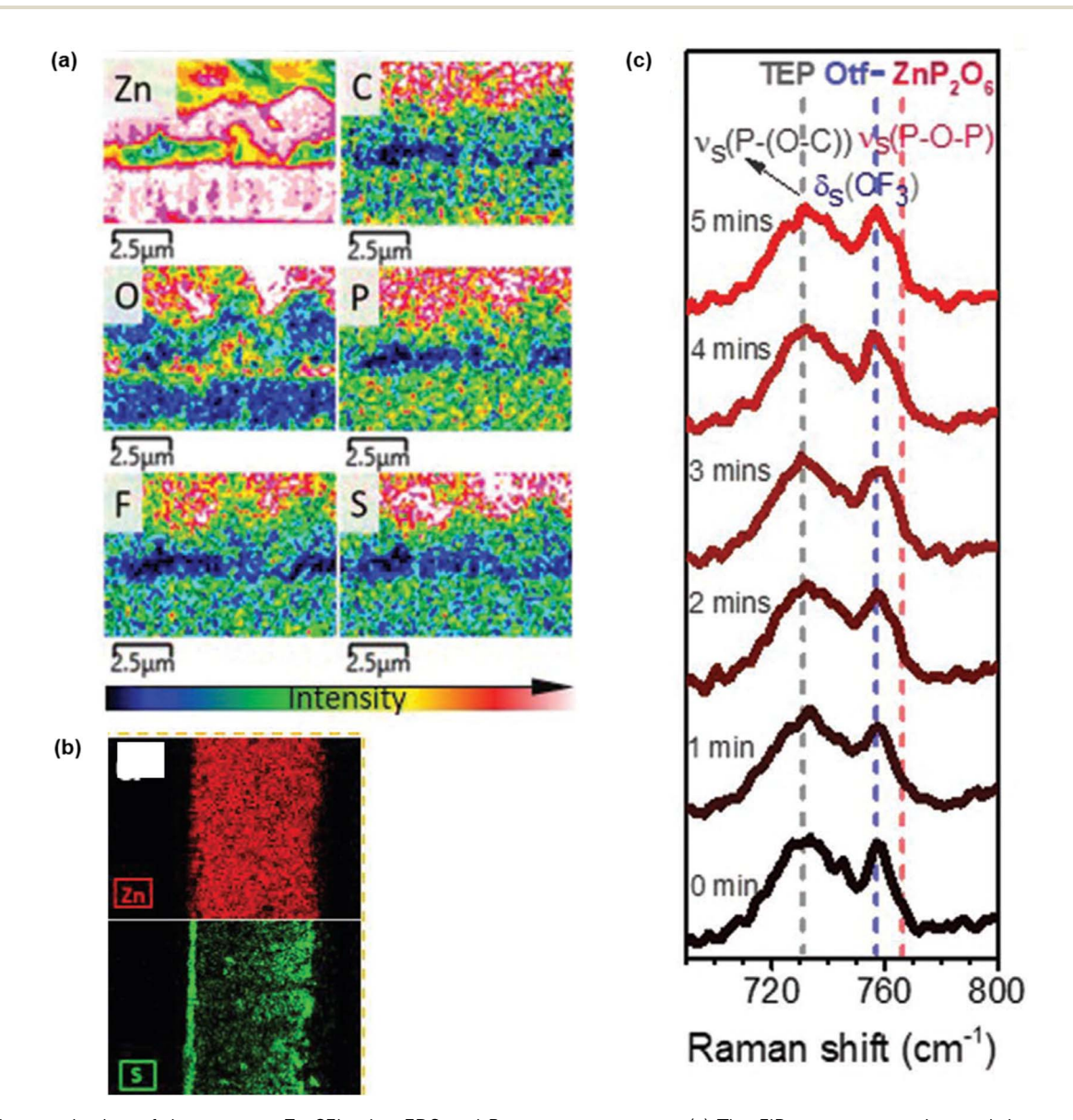


Fig. 11 Characterization of the aqueous Zn SEI using EDS and Raman spectroscopy. (a) The FIB-cut cross-section and the corresponding elemental distribution from EDS after cycling in  $Zn(OTf)_2$ -TEP- $H_2O$  electrolyte. Reproduced from ref. 64, Copyright 2021 Wiley VCH. (b) EDS mapping of Zn element (top) and S element (bottom). Reproduced from ref. 123, Copyright 2020 Wiley VCH. (c) In situ Raman spectra of the Zn(OTf)<sub>2</sub>-TEP-H<sub>2</sub>O electrolyte on the Zn surface within different ranges. Reproduced from ref. 64, Copyright 2021 Wiley VCH.

chemical composition characterization on the zinc anode are XRD and XPS. XRD is used to characterize the crystalline structures in the SEI, which are mainly for inorganic components, while XPS is used to determine the binding energy between elements on the surface of the SEI up to 10 nm, indicating the bonding and functional groups in the SEI. Wang et al.26 used XRD and XPS to characterize a Zn12(SO4)3-Cl<sub>3</sub>(OH)<sub>15</sub>·5H<sub>2</sub>O, ZnSO<sub>3</sub>, and ZnS enriched-SEI formed in a 1.3 m ZnCl<sub>2</sub>/H<sub>2</sub>O-dimethyl sulfoxide (DMSO, volume ratio of  $H_2O/DMSO = 4.3:1$ ) electrolyte. The stable and robust SEI can prevent Zn dendrite formation and suppress water decomposition in aqueous Zn metal batteries. As shown in the XRD patterns (Fig. 9a), obvious peaks for Zn<sub>12</sub>(SO<sub>4</sub>)<sub>3</sub>Cl<sub>3</sub>(OH)<sub>15</sub>·5H<sub>2</sub>O and Zn<sub>5</sub>(OH)<sub>6</sub>(CO<sub>3</sub>)<sub>2</sub> are observed in the cycled zinc anode with the ZnCl<sub>2</sub>-H<sub>2</sub>O-DMSO electrolyte, indicating they are two major components in the Zn<sup>2+</sup> conductive SEI, while Zn<sup>2+</sup>-insulating Zn<sub>5</sub>(OH)<sub>8</sub>Cl<sub>2</sub>·H<sub>2</sub>O is identified as the major component in the SEI generated by the ZnCl<sub>2</sub>-H<sub>2</sub>O electrolyte. To further understand the structure of the SEI formed in the ZnCl<sub>2</sub>-H<sub>2</sub>O-DMSO electrolyte, XPS with Ar+ sputtering depth profiling was employed. The results in Fig. 10a show that inorganic ZnSO<sub>3</sub>, ZnSO<sub>4</sub>, and ZnS with minor organic S-C species are major components in the top surface of the SEI formed by the 1.3 m ZnCl<sub>2</sub>/H<sub>2</sub>O-DMSO electrolyte before Ar<sup>+</sup> sputtering. To analyze the inner structure of the SEI, Ar<sup>+</sup> sputtering was used, confirming that Zn<sub>12</sub>(SO<sub>4</sub>)<sub>3</sub>Cl<sub>3</sub>(OH)<sub>15</sub>·5H<sub>2</sub>O, ZnSO<sub>3</sub>, and ZnS are

major components in the SEI. The solvation structure of  $Zn^{2+}$  with DMSO contributes to the formation of  $Zn^{2+}$  conductive  $Zn_{12}(SO_4)_3Cl_3(OH)_{15} \cdot 5H_2O$ ,  $ZnSO_3$ , and ZnS enriched SEI.

Guo *et al.*<sup>64</sup> introduced a fire-retardant, TEP, with a high Gutmann donor number of 26 kcal  $\mathrm{mol}^{-1}$  to form a nonaqueous/aqueous hybrid electrolyte for RZMBs. The optimized 0.5 m  $\mathrm{Zn}(\mathrm{OTf})_2/\mathrm{TEP}:\mathrm{H_2O}$  (TEP:  $\mathrm{H_2O}$  volume ratio of 1:1) electrolyte (denoted as  $\mathrm{Zn}(\mathrm{OTf})_2-\mathrm{TEP}-\mathrm{H_2O}$ ) leads to a polymeric-inorganic (poly- $\mathrm{ZnP_2O_6}$  and  $\mathrm{ZnF_2}$ ) species-containing SEI with a low electrical conductivity and a low activation energy barrier for  $\mathrm{Zn}^{2+}$  diffusion. To understand the SEI chemistries, XPS (Fig. 10b) was carried out to prove the formation of the polymetaphosphate (poly- $\mathrm{ZnP_2O_6}$ ) from the decomposition of the TEP solvent. Some inorganic components such as  $\mathrm{ZnF_2}$ , carbonates, and sulfur compounds from the decomposition of the anions were also observed by XPS.

The aqueous  $Zn(OTf)_2$  electrolyte with 0.5 m  $Me_3EtN-OTf$  as an additive increases the Zn plating/stripping CE from 87.6% to 99.9% by forming a fluorinated and hydrophobic interphase that conducts  $Zn^{2+}$  but suppresses the side reaction.  $^{31}$  XPS was employed to analyze the chemical structure of the SEI. The sharp peak for inorganic  $ZnF_2$  is detected at  $\sim$ 684.7 eV in the XPS spectrum (Fig. 10c). The peak ratio of  $ZnF_2$  to  $CF_3$  increases after sputtering, confirming the  $ZnF_2$ -rich SEI structure. In addition to  $ZnF_2$ , the C 1s spectrum (Fig. 10d) indicates that  $ZnCO_3$  is also a main component in the SEI, which could also

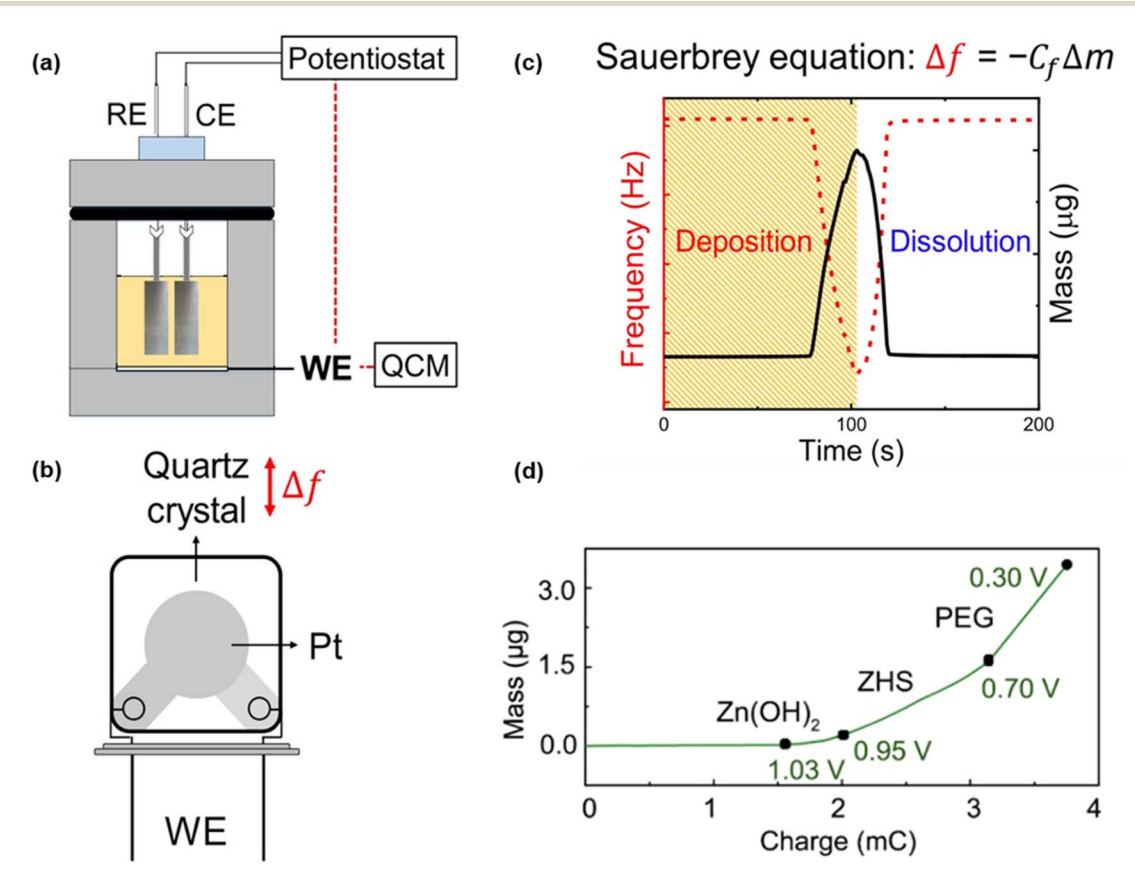


Fig. 12 A schematic of EQCM analysis. (a) EQCM cell, (b) quartz crystal working electrode, and (c) exemplary frequency and mass profiles during the Zn stripping/plating process. Reproduced from ref. 138, Copyright 2021 American Chemical Society. (d) Mass vs. charge curve from EQCM on a Zn SEI when 1.0 m ZnSO<sub>4</sub> – 1000 ppm PEG electrolyte was used. Reproduced from ref. 139, Copyright 2020 American Chemical Society.

contribute to the high CE. The trace amount of nitrogen in the SEI may be from Zn(OH)<sub>2</sub>(Me<sub>3</sub>N)<sub>2</sub>, which is from the decomposition of the alkylammonium via a Hofmann elimination.

XRD and XPS are also feasible to characterize the artificial SEI. Hao et al. 123 deposited a robust and homogeneous ZnS interphase on the Zn surface by a vapor-solid strategy. The artificial ZnS layer obtained at 350 °C enables the side reactionfree and dendrite-free zinc anode's use in high-performance aqueous RZMBs. As shown in Fig. 9b, the XRD pattern shows new peaks at 28.6°, 47.5°, and 56.3°, representing the (111), (200), and (311) planes of ZnS. XPS (Fig. 10e) is used to confirm the formation of Zn-S polar bonds at the interphase of ZnS and zinc metal.

4.1.1.2 EDS. EDS, typically coupled with either SEM or TEM, is an X-ray microanalysis technique to obtain the distributions

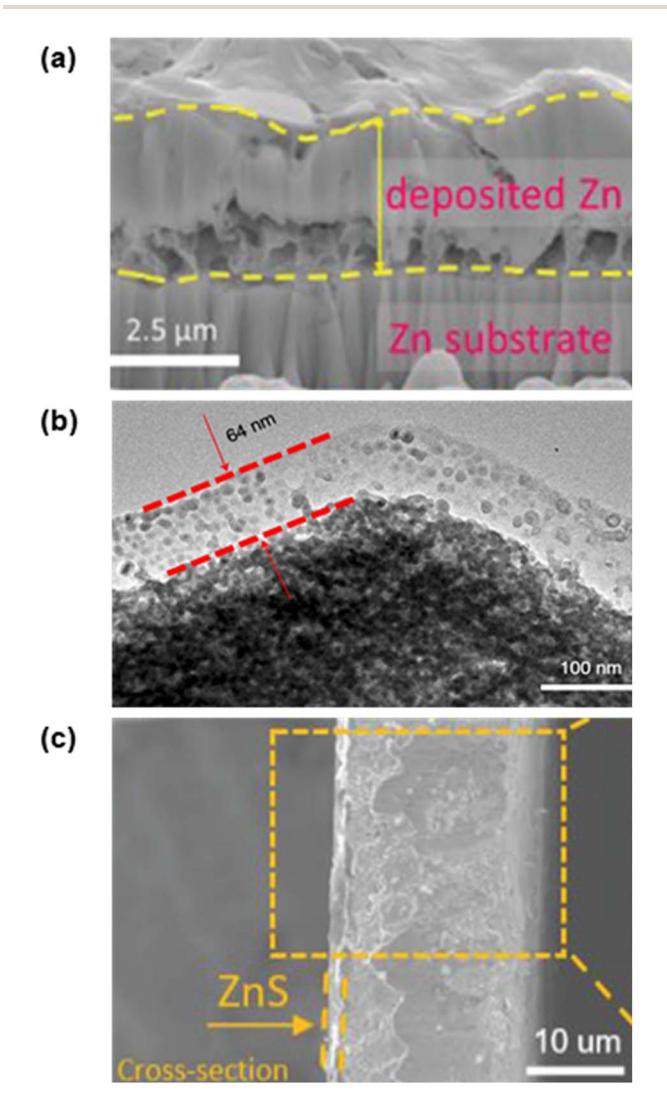


Fig. 13 Characterization of the aqueous Zn SEI using SEM and TEM. (a) The FIB-cut cross-section SEM image on a Zn anode after cycling in Zn(OTf)<sub>2</sub>-TEP-H<sub>2</sub>O electrolyte. Reproduced from ref. 64, Copyright 2021 Wiley VCH. (b) TEM image of the cycled Zn anode surface in 4 m Zn(OTF)<sub>2</sub> + 0.5 m Me<sub>3</sub>EtN-OTF. Reproduced from ref. 31, Copyright 2021 Springer Nature. (c) Cross-sectional SEM image of ZnS@Zn foil, showing that the thickness of the ZnS is  $\approx 0.5 \mu m$ . Reproduced from ref. 123, Copyright 2020 Wiley VCH.

and content of the selected elements across a sample. This technique has been successfully applied to evaluate both in situ formed or artificial SEI elements to supplement other surface techniques such as XPS. According to Liu et al.64 and Hao et al., 123 the EDS mapping (Fig. 11a and b) shows consistent results with XPS for poly-ZnP<sub>2</sub>O<sub>6</sub> and ZnS chemistries, respectively.

4.1.1.3 Raman spectroscopy. Adopting lasers as the excitation source, Raman spectroscopy can be used to determine the molecular structure by studying the vibrations of functional groups in SEI components. As demonstrated by Liu et al.,64 Raman spectroscopy (Fig. 11c) was carried out to prove the formation of the polymetaphosphate (poly-ZnP<sub>2</sub>O<sub>6</sub>) from the decomposition of the TEP solvent.

4.1.1.4 EQCM. As a complementary method to understand chemical compositions change, EQCM is a powerful technique to study SEI formation on the zinc metal anode. Fig. 12a and b show the schematic diagrams of the setup for EQCM analysis, which is widely used to detect the change in the mass of the electrode during electrochemical processes. According to the Sauerbrey equation  $(\Delta f = -C_f \Delta m)$ , there is a linear dependence of characteristic frequency on the mass of the crystal oscillator. The vibrational frequency of the quartz crystal decreases as the weight of the working electrode increases (Fig. 12c), providing information about the structure of the newly formed products. To offer more nucleation sites for dendrite regulation, the well-studied polyethylene glycol (PEG) is used as an electrolyte additive to promote Zn plating and stripping. Chen et al.139 used EQCM to precisely detect the components and dynamic evolution of byproducts upon cycling. According to their EQCM results (Fig. 12d), a small amount of interfacial byproducts of Zn(OH)2 and zinc hydrogen sulfate Zn<sub>4</sub>(OH)<sub>6</sub>SO<sub>4</sub>·5H<sub>2</sub>O (ZHS) is formed when the potential is above 0.7 V. The adsorption of PEG on the Zn anode occurs at a potential below 0.7 V.

## 4.1.2 Characterization of SEI morphology

4.1.2.1 SEM and TEM. SEM and TEM, coupled with FIB for sample preparation, are the most common techniques to characterize SEI morphology in aqueous RZMBs. EDS and electron energy loss spectroscopy (EELS) are typically performed together to confirm the SEI region in the SEM or TEM images. Using FIB and SEM, Liu et al. 64 illustrated that the Zn(OTf)2-TEP-H<sub>2</sub>O electrolyte enables uniform and dense Zn deposition (Fig. 13a), and the SEI contains the elements of Zn, C, O, P, F, and S (Fig. 11a). Leveraging TEM, Cao et al.31 clearly revealed the thickness of the SEI of 64 nm derived from the 4 m Zn(OTf)<sub>2</sub> + 0.5 m Me<sub>3</sub>EtN-OTf + H<sub>2</sub>O electrolyte, while no such SEI was formed in the 4 m  $Zn(OTf)_2 + H_2O$  electrolyte (Fig. 13b). The artificial SEI layer can also be visualized by SEM. Hao et al.123 showed that the zinc surface is evenly covered by an artificial ZnS layer, which is also confirmed by EDS mapping of the cross section (Fig. 11b and 13c). The cross-sectional image shows a homogeneous ZnS layer on the Zn surface with a thickness of  $\sim$ 0.5  $\mu$ m.

As a passing note, the thickness of the SEI (<50 nm) in nonaqueous LIBs is typically beyond the detection limit of SEM.128 The feasibility of using SEM here is due to the abnormal

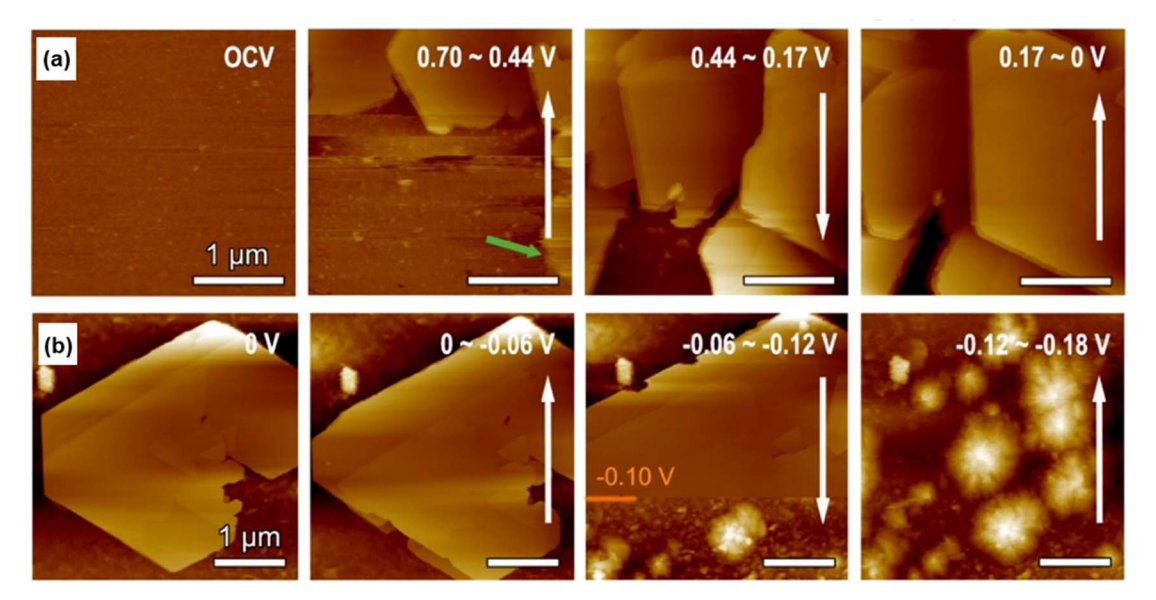


Fig. 14 Characterization of the aqueous Zn SEI using AFM. (a and b) In situ potential-dependent AFM topography images of the Zn SEI when 1.0 M ZnSO<sub>4</sub>-1000 ppm PEG electrolyte was used. The data scale in the AFM image is 300 nm. Reproduced from ref. 139, Copyright 2020 American Chemical Society.

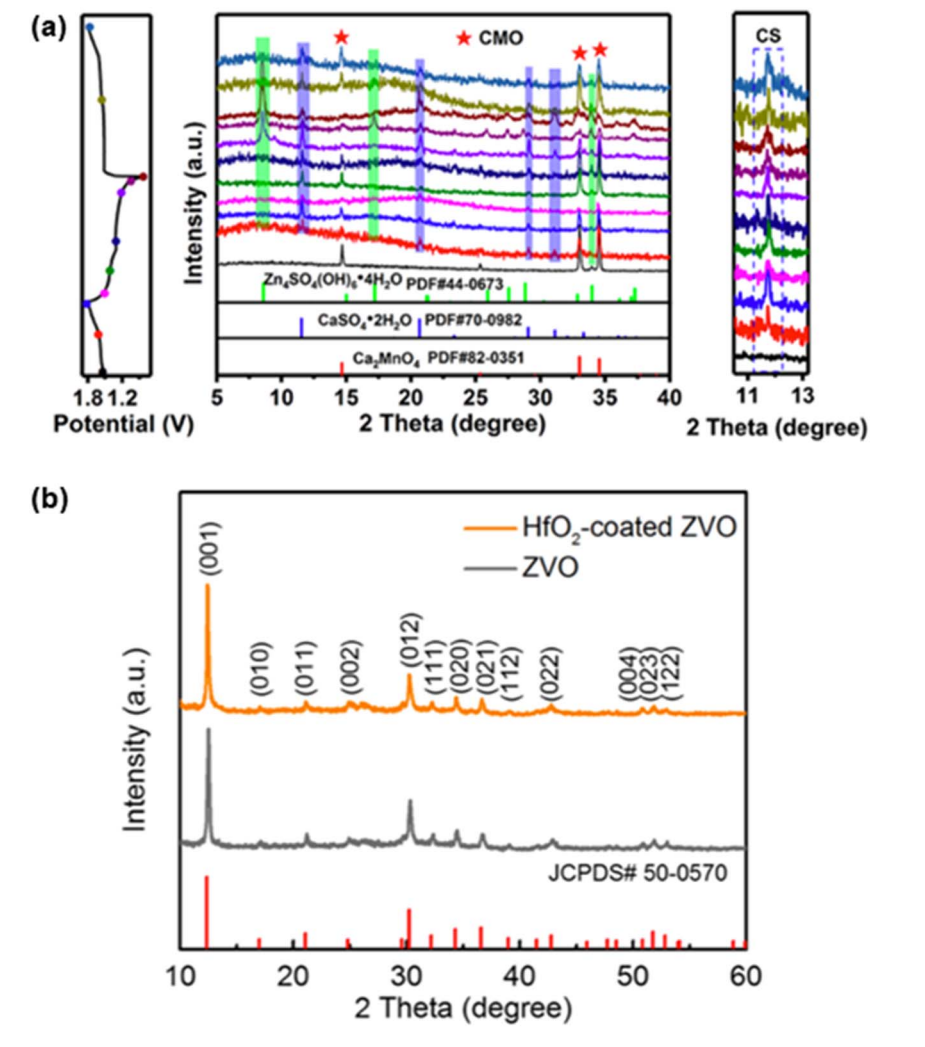
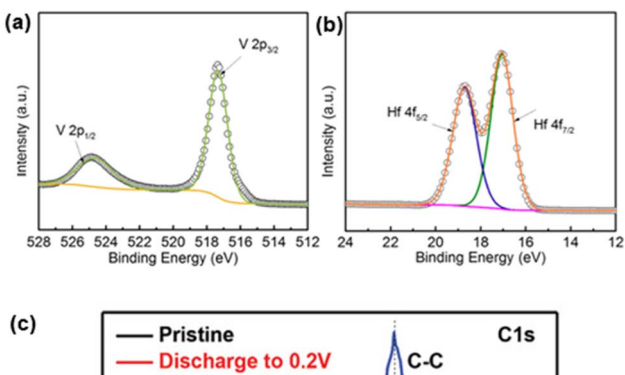


Fig. 15 Characterization of the aqueous Zn CEI using XRD. (a) Ex situ XRD of the first two cycles for a  $Ca_2MnO_4$  cathode. Reproduced from ref. 42, Copyright 2019 American Chemical Society. (b) XRD pattern showing that the HfO<sub>2</sub> CEI coating does not change the  $Zn_3V_2O_7 \cdot 2H_2O$  cathode structure. Reproduced from ref. 44, Copyright 2019 American Chemical Society.



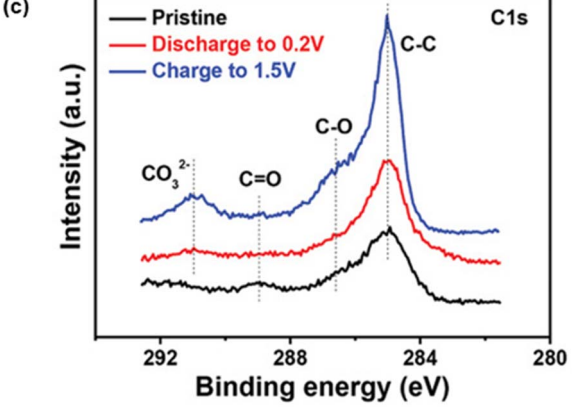


Fig. 16 Characterization of the aqueous Zn CEI using XPS. (a and b) XPS high-resolution spectra of (a) V 2p and (b) Hf 4f obtained from a HfO2-coated Zn3V2O7·2H2O cathode. Reproduced from ref. 44, Copyright 2019 American Chemical Society. (c) XPS high-resolution spectra of C 1s obtained from a hydrated sodium strontium vanadate cathode upon the 1st discharge-charge process at selected states with 0.5 A g<sup>-1</sup> current density. Reproduced from ref. 120, Copyright 2021 Wiley VCH.

thickness of the SEI and unclear SEI evolution mechanisms in aqueous electrolytes.

4.1.2.2 AFM. Due to a high spatial resolution, the AFM technique has been widely used to understand the morphology changes of Zn anodes under electrochemical environments. It can also be used to study the dynamic evolution of SEI morphology. According to Chen et al., 139 Zn deposits with more nucleation sites and a much smoother surface in the 1 M ZnSO<sub>4</sub> - 1000 ppm PEG electrolyte, enabling a compact dendrite-free morphology. In situ AFM is used to monitor the morphology of PEG adsorption on the Zn anode during the discharge. As shown in Fig. 14a and b, the PEG adsorption orients in parallel, and the PEG lamellas cover the electrode surface, acting as a physical barrier to prevent the parasitic reaction between zinc metal and water. As the potential further decreases, the lamellar PEG grows larger, preventing Zn dendrite growth.

Since the SEI is vital for the reversibility of Zn plating/stripping, mitigation of dendrite growth, and protection from parasitic reactions between Zn metal and water, the rational design of a Zn-ion conductive, uniform, stable and robust SEI is the key for high-performance aqueous Zn batteries. The extensive characterization techniques discussed in this section provide a fundamental understanding toward the structures and properties of the SEI, benefiting further optimization of aqueous electrolytes and artificial SEI to achieve a stable and robust interphase in aqueous RZMBs. More in situ techniques, such as operando reflection interference microscopy, 140 are required to further understand the dynamic formation mechanism of the SEI and its physicochemical properties to realize the practical applications of aqueous RZMBs. Moreover, the advanced SEI characterization techniques for aqueous Zn batteries may also be applicable for other energy storage devices to investigate the interfacial structures and improve the battery performance.

#### 4.2 Characterization of CEI

To date, considerable efforts have been devoted to developing and characterizing the SEI on the zinc metal anode, because it not only widens the electrochemical stability window of the electrolytes but also improves the battery cycle life. Significant progress was achieved in addressing the challenges in the anode and obtaining a dendrite-free and stable Zn metal anode. However, another common challenge in RZMBs is the cathode material dissolution, which results in fast capacity decay upon cycling. To circumvent this challenge, it is critical to study the structure of the protective interphase in the cathode, known as the CEI. It is generated by the decomposition and reaction of the electrolytes in the interface between the cathode and the electrolyte at a high working voltage. Due to the similarity of the CEI to the SEI, characterization techniques for the SEI are extensively used to investigate the structure of the CEI. Based on the fundamental understanding of the interfacial structure in the cathode, it is feasible to rationally design an ionically conductive and electronically insulating CEI with superior chemical and electrochemical stability in the high voltage window to mitigate cathode material dissolution and obtain stable cathodes for high-performance RZMBs.

## 4.2.1 Characterization of CEI chemical compositions

4.2.1.1 XPS and XRD. XPS and XRD are also the common techniques used for characterizing CEI chemistries. Zhou et al.42 discovered that in situ formation of a CaSO4 · 2H2O-based single component CEI in RZMBs with a Ca2MnO4 cathode and a 2 mol ZnSO<sub>4</sub> + 0.1 mol MnSO<sub>4</sub> electrolyte prevented manganese dissolution. As shown in Fig. 15a, ex situ XRD indicates the generation of CaSO<sub>4</sub>·2H<sub>2</sub>O during charging, and it remains stable upon subsequent discharge. Meanwhile, a common byproduct of Zn<sub>4</sub>SO<sub>4</sub>(OH)<sub>6</sub>·4H<sub>2</sub>O is also formed during the discharge, but it disappears during charging. The crystalline structure of Ca<sub>2</sub>MnO<sub>4</sub> remains unchanged after the discharge and charging, demonstrating a stable cathode in RZMBs.

In addition to the *in situ* formation of the CEI on the cathode by the decomposition of electrolytes, another method to stabilize the cathode is the construction of an artificial CEI. Alshareef et al.44 employed an ALD technique to uniformly and conformally deposit an ultrathin (5 nm) HfO2 film as the CEI on the surface of the Zn<sub>3</sub>V<sub>2</sub>O<sub>7</sub>·2H<sub>2</sub>O cathode. The HfO<sub>2</sub>-based artificial CEI not only reduces the generation of the  $Zn_4SO_4(OH)_6 \cdot xH_2O$ byproduct in the CEI but also suppresses the dissolution of the cathode material in the electrolyte (1 M ZnSO<sub>4</sub> in water). In the XRD results (Fig. 15b), the HfO<sub>2</sub>-coated Zn<sub>3</sub>V<sub>2</sub>O<sub>7</sub>·2H<sub>2</sub>O cathode

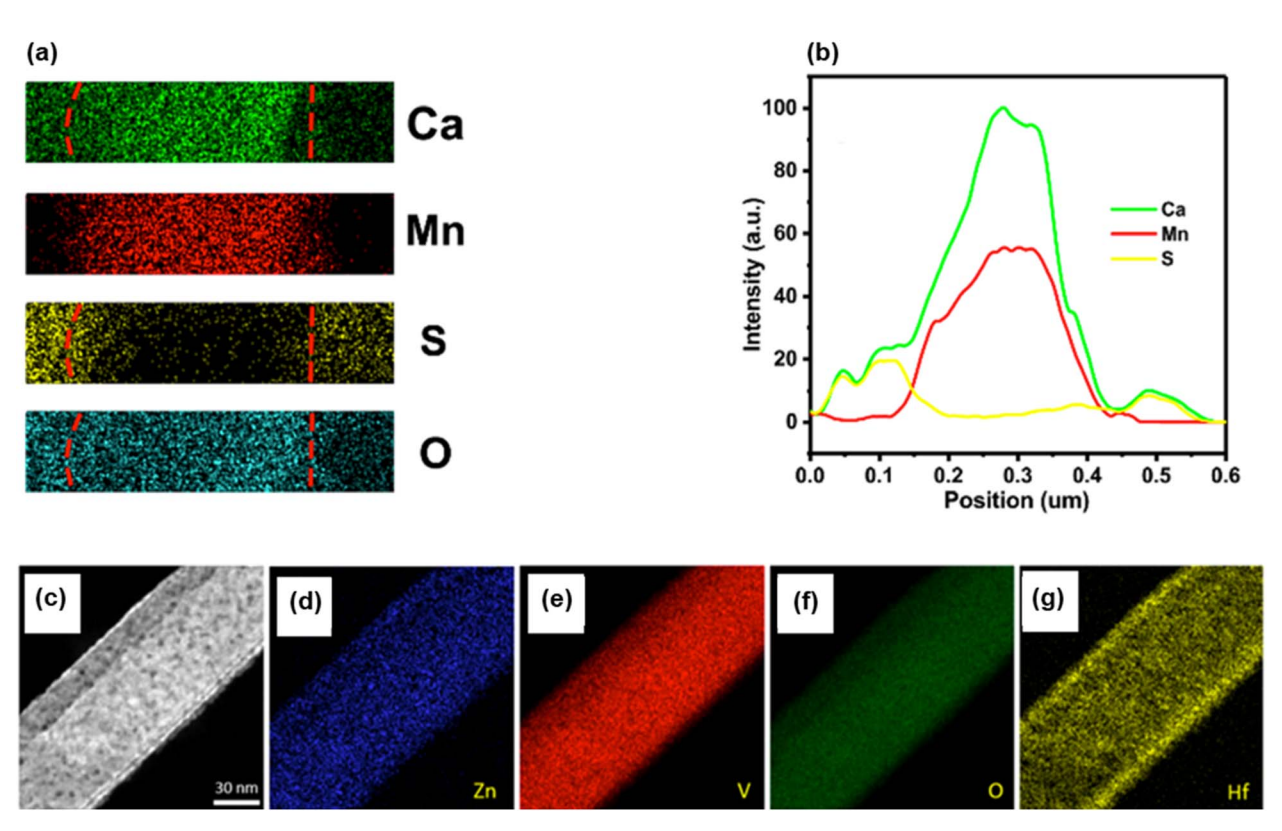


Fig. 17 Characterization of the aqueous Zn CEI using EDS. (a) EDS mapping graph of the  $Ca_2MnO_4$  electrode at the fully charged state. (b) The linear EDS scan of the  $Ca_2MnO_4$  electrode at the fully charged state. Reproduced from ref. 42, Copyright 2019 American Chemical Society. (c-g) TEM-EDS elemental maps of a  $HfO_2$ -coated  $Zn_3V_2O_7 \cdot 2H_2O$  individual nanobelt. Reproduced from ref. 44, Copyright 2019 American Chemical Society.

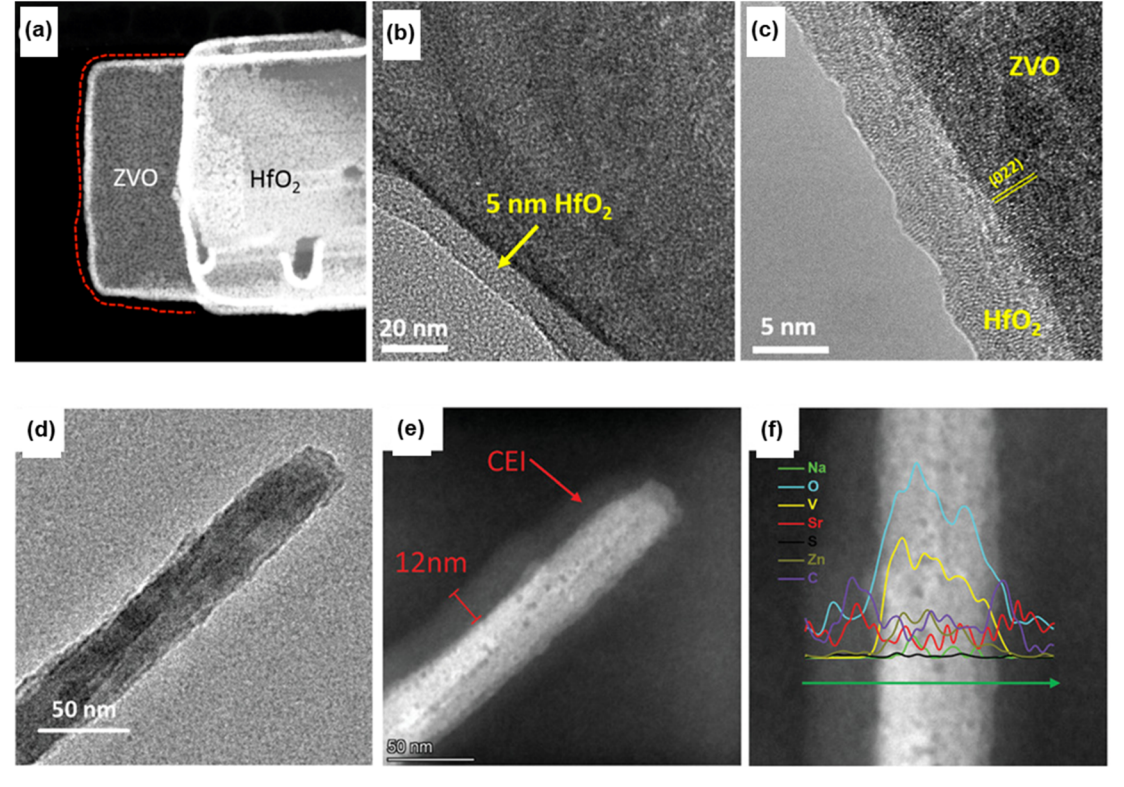


Fig. 18 Characterization of the aqueous Zn CEI using TEM. (a) HAADF-STEM image, (b) TEM image, and (c) HR TEM image of a  $HfO_2$ -coated  $Zn_3V_2$ - $O_7 \cdot 2H_2O$  cathode. Reproduced from ref. 44, Copyright 2019 American Chemical Society. (d) TEM image, (e) HAADF image, and (f) HAADF image with the green line showing the EDS line scanning path for the hydrated sodium strontium vanadate cathode. Reproduced from ref. 120, Copyright 2021 Wiley VCH.

exhibits the same XRD pattern as the Zn<sub>3</sub>V<sub>2</sub>O<sub>7</sub>·2H<sub>2</sub>O cathode without coating, demonstrating the ultrathin HfO2 film is an amorphous phase and does not impact the crystalline structure of the cathode material. XPS (Fig. 16a and b) further confirms that the chemical valence of vanadium is not affected by the HfO<sub>2</sub> coating, while Hf-O bonding in the HfO<sub>2</sub> can be observed.

Another example of using an artificial CEI to prevent vanadium dissolution in aqueous RZMBs is reported by Miao et al. 120 An in situ artificial CEI strategy is proposed to convert soluble Sr(OH)2 to insoluble SrCO3 as the CEI coating layer on the vanadium-based cathode. In the XPS results, the appearance of a new peak for  $CO_3^{2-}$  is clearly observed, indicating the formation of SrCO<sub>3</sub> on the surface (Fig. 16c).

4.2.1.2 EDS. The use of EDX with either a linear scan or mapping mode is able to visualize elemental distribution across the CEI. Zhou et al.42 in situ coated a Ca2MnO4 cathode with a CEI layer of CaSO<sub>4</sub>·2H<sub>2</sub>O. Combining both the EDX mapping graph (Fig. 17a) and linear scan (Fig. 17b) showed that there is more S on the surface while more Mn is present in the center, confirming the core-shell structure. Alshareef et al.44 successfully characterized an HfO2-coated Zn3V2O7·2H2O cathode and confirmed its core-shell structure by using EDS elemental mapping in Fig. 17c-g, where Zn, V, O, and Hf elements are homogeneously distributed in the HfO2-coated Zn3V2O7·2H2O nanobelt.

4.2.2 Characterization of CEI morphology. Coupled with EDX or EELS, TEM is still the most common technique to visualize the CEI formed in aqueous RZMBs. Alshareef et al.44 used high angle annular dark-field scanning TEM (HAADF-STEM) and high-resolution (HR) TEM (Fig. 18a-c) to characterize the morphology and showed the core-shell structure of the HfO2-coated Zn3V2O7·2H2O. A uniform HfO2 layer with a thickness of 5 nm was on the Zn<sub>3</sub>V<sub>2</sub>O<sub>7</sub>·2H<sub>2</sub>O nanobelt. Miao et al.120 used ex situ TEM, HAADF, and EDS (Fig. 18d-f) to prove the in situ coating strategy of coating a SrCO<sub>3</sub> CEI layer on the vanadium-based cathode. A CEI layer with a thickness of over 10 nm can be observed in the HAADF images of the cycled cathode.

Analogous to the SEI in the anode, the CEI in the cathode is also critical for the development of low-cost and high-performance RZMBs. More advanced characterization techniques such as cryo-TEM, etc. are required to fully understand the structure and formation mechanism of the CEI. Based on the fundamental understanding, the guidance for rational design of the CEI can be achieved to address the challenges in the cathodes of RZMBs for practical applications.

#### 5. Conclusions and perspective

#### 5.1 Conclusions

To avoid a potential resource crisis (e.g. lithium, cobalt, nickel) in the future, it is urgent to advance the development of rechargeable aqueous RZMBs as a complementary battery system to LIBs. Significant progress has been made by extending cyclability with more choices of electrodes and electrolytes for RZMBs. However, the commercialization of aqueous RZMBs still requires further improvement on electrochemical

performance, including in terms of energy density, cycling lifetime, storage lifetime, compatibility with different temperatures, and low cost. As bridges connecting electrodes and electrolytes, optimal interphases in RZMBs, including both the SEI and CEI, are urgently required to advance this technology.

In this review, we systematically examined the in situ formation process of both the SEI and CEI in aqueous RZMBs with different co-solvents, additives, or salts. Typically, these electrolyte components affect interphases by entering the EDL with or without decomposition. Such a decomposition process can undergo either a chemical or an electrochemical process to leave a layer of chemical signature on the electrode surface. Most literature studies revealed that electrolyte components with the EDL tend to adsorb on the electrode surface instead of decomposing to screen out water molecules and homogenize Zn<sup>2+</sup> transport. The artificial fabrication processes of the SEI and CEI were also discussed. These strategies, including application of inorganic compound coatings, polymeric coatings, and metallic or MOF coatings, impart unique characteristics to the electrode-electrolyte interphase in the aqueous media thereby preventing side reactions such as water decomposition and TM dissolution. According to the latest experimental observations, there is no universal model that can be used to describe SEI or CEI structures since they are determined by the electrolyte components or artificial fabrication chemistries. Consequently, the properties of the SEI or CEI such as Zn<sup>2+</sup> ionic conductivity, mechanical properties, thermal stability, and chemical and electrochemical stability vary due to different SEI or CEI structures and chemistries. In fact, these properties determine the battery performances. It is important to unravel the properties of these SEIs or CEIs for rational design and optimization of their functions.

## 5.2 Perspective

Despite the remarkable progress that has been achieved in the interphase studies of aqueous RZMBs, there remain many challenges in understanding the SEI/CEI and correlating SEI/ CEI properties to battery performances. Therefore, we propose our perspective on future studies on the SEI/CEI for developing high-performance aqueous RZMBs.

5.2.1 Better understanding on how SEI/CEI evolves as a function of time. The continuous evolution of the SEI in nonaqueous electrolytes of LIBs is inevitable due to the electron tunneling effect.24 To explain such a growth, a simple model of diffusion-limitation was adopted (eqn (1)), which has been confirmed by Dahn et al. experimentally141

$$\frac{\mathrm{d}x}{\mathrm{d}t} = \sqrt{\frac{k}{2}}t^{-1/2} \tag{1}$$

where x is the hypothetical thickness of an ideal SEI, t is the time, dx/dt is the SEI growth rate, and k is a constant which depends on electrolytes/electrodes and temperature. Here, the SEI also needs to (1) have homogeneous components across the whole layer and (2) be uniform without any defects (e.g. cracks, holes).

Considering that water is one of the most powerful solvents, due to its high dielectric constant and dipole moment, an aqueous SEI/CEI evolution during cell operation or storage could suffer from more complex processes and severe challenges compared to its non-aqueous counterpart. Additionally, SEI/CEI components could have higher solubility issues in an aqueous electrolyte compared to non-aqueous electrolytes, which could result in the formation of defects, accelerate irreversible reactions, and require an SEI/CEI repair. It is important to understand SEI/CEI evolution as a function of time in aqueous electrolytes in the future.

5.2.1.1 Development of new methods. The real structure and chemical composition of the SEI/CEI immersed in aqueous electrolytes, especially as a function of time, are still not yet completely understood due to the limitation of characterization methods. Therefore, operando techniques with multi-modality chemical imaging and spectroscopy are of high interest to track the SEI/CEI evolution chemically and structurally. Currently, TEM coupled with EELS and EDS is the most widely used method. However, electron beams and X-rays could damage the SEI/CEI when overexposure occurs. For this reason, nondestructive characterization approaches should be developed and applied. In addition, the development of computational methods will help elucidate the evolution mechanisms and properties of the SEI/CEI at the atomistic and molecular levels, providing supporting explanations of complex phenomena observed experimentally.

5.2.1.2 pH. Aqueous electrolytes with a wide pH range, from acidic to basic, have been investigated for RZMBs. However, it is still unclear how protons or hydroxide anions affect SEI/CEI evolution, especially the chemical reaction between protons and Zn that can occur where SEI defects exist. For this reason, the analysis of SEI/CEI evolution in aqueous electrolytes at different pH levels should be performed structurally and chemically.

5.2.1.3 Temperature. In most of the current reports, RZMB testing and relevant analysis are usually performed under room temperature conditions. As a promising candidate for future grid energy storage, RZMBs will likely suffer from either high or low temperature conditions. It is important to widen their testing temperature range to enhance the practical utilization of aqueous RZMBs. Consequently, the analysis of SEI/CEI evolution across a wide temperature range is key to tailoring interphasial properties to meet different temperature requirements.

5.2.2 Correlation of SEI/CEI studies with cell energy density. Due to the unique advantage of volumetric energy density of Zn metal anodes, it is important to increase the Zn utilization per cycle (>50%) to fully realize such an advantage. However, most current SEI studies were performed when limited Zn utilization per cycle (typically <2%) was used. Higher Zn utilization per cycle could generate more mechanical stress on the SEI. For this reason, the analysis of SEI evolution at higher Zn utilization per cycle needs to be carried out.

**5.2.3** Correlation of SEI/CEI studies with cell lifetime. In addition to proton contribution to the cell capacity, the Zn inventory in the cell is the resource of the reversible capacity, and its retention is directly correlated with cell lifetime. Typically, Zn inventory loss comes from SEI/CEI formation,

evolution, or repair. To facilitate the manufacturing process of aqueous RZMBs in the future, it would be easier to use Zn powder instead of Zn foil. Due to the increased surface area, it is worth fully understanding the SEI evolution with potential Zn inventory loss in the future.

5.2.3.1 Cycling lifetime. CE is an important parameter to characterize Zn inventory loss during cell cycling. According to Dahn *et al.*,<sup>143</sup> CE is a function of cycling time instead of cycle number. Most current reports demonstrate excellent CEs with a high cycling rate, which could hide the real Zn inventory loss process. To correlate SEI/CEI studies with cell lifetime, it is important to accurately quantify Zn inventory loss with a low rate (*e.g.* C/20) to allow a complete parasitic reaction process in the future.

5.2.3.2 Calendar lifetime. As a standard testing procedure for non-aqueous LIBs, high temperature storage testing has rarely been performed for aqueous RZMBs to characterize their calendar lifetime performance. It is critical to correlate SEI/CEI studies with storage testing results to fully understand the effect of SEI/CEI quality on cell gas evolution, Zn inventory loss, and voltage decay during the open circuit voltage resting process, especially at high temperatures. This is essential to accelerate the wide commercialization of aqueous RZMBs.

## Conflicts of interest

There are no conflicts to declare.

## Acknowledgements

This work was supported, in part, by funds provided by the University of North Carolina at Charlotte. J. X. and L. M. acknowledge the support by the Ignite Planning Grant Program at UNC Charlotte. C. L. acknowledges the support by the US National Science Foundation Award No. 2000102.

## Notes and references

- 1 G. Bridge and E. Faigen, Towards the Lithium-Ion Battery Production Network: Thinking Beyond Mineral Supply Chains, *Energy Res. Soc. Sci.*, 2022, **89**, 102659.
- 2 A. Volta, XVII. On the Electricity Excited by the Mere Contact of Conducting Substances of Different Kinds. In a Letter from Mr Alexander Volta, F. R. S. Professor of Natural Philosophy in the University of Pavia, to the Rt. Hon. Sir Joseph Banks, Bart. K.B. P. R. S, *Philos. Trans. R. Soc. London*, 1800, **90**, 403–431.
- 3 L. E. Blanc, D. Kundu and L. F. Nazar, Scientific Challenges for the Implementation of Zn-Ion Batteries, *Joule*, 2020, 4, 771–799.
- 4 J. Song, K. Xu, N. Liu, D. Reed and X. Li, Crossroads in the Renaissance of Rechargeable Aqueous Zinc Batteries, *Mater. Today*, 2021, 45, 191–212.
- 5 M. H. Askar, H. Abbas and S. E. Afifi, Rechargeability of Manganese Dioxide/Zinc Cell Using Zinc Sulfate Electrolyte, *J. Power Sources*, 1994, **48**, 303–309.

- 6 S. H. Kim and S. M. Oh, Degradation Mechanism of Layered MnO<sub>2</sub> Cathodes in Zn/ZnSO<sub>4</sub>/MnO<sub>2</sub> Rechargeable Cells, J. Power Sources, 1998, 72, 150-158.
- 7 D. Kundu, B. D. Adams, V. Duffort, S. H. Vajargah and L. F. Nazar, A High-Capacity and Long-Life Aqueous Rechargeable Zinc Battery Using a Metal Oxide Intercalation Cathode, Nat. Energy, 2016, 1, 16119.
- 8 P. Senguttuvan, S.-D. Han, S. Kim, A. L. Lipson, S. Tepavcevic, T. T. Fister, I. D. Bloom, A. K. Burrell and C. S. Johnson, A High Power Rechargeable Nonaqueous Multivalent Zn/V<sub>2</sub>O<sub>5</sub> Battery, Adv. Energy Mater., 2016, 6, 1600826.
- 9 M. Liao, J. Wang, L. Ye, H. Sun, Y. Wen, C. Wang, X. Sun, B. Wang and H. Peng, A Deep-Cycle Aqueous Zinc-Ion Battery Containing an Oxygen-Deficient Vanadium Oxide Cathode, Angew. Chem., Int. Ed., 2020, 59, 2273-2278.
- 10 P. Hu, et al., Highly Durable Na2v6o16·1.63h2o Nanowire Cathode for Aqueous Zinc-Ion Battery, Nano Lett., 2018, 18, 1758-1763.
- 11 L. Ma, et al., High-Efficiency Zinc-Metal Anode Enabled by Liquefied Gas Electrolytes, ACS Energy Lett., 2021, 6, 4426-
- 12 L. Wang, M. Jiang, F. Liu, Q. Huang, L. Liu, L. Fu and Y. Wu, Layered TiS2 as a Promising Host Material for Aqueous Rechargeable Zn Ion Battery, Energy Fuels, 2020, 34, 11590-11596.
- 13 L. Zhang, L. Chen, X. Zhou and Z. Liu, Towards High-Voltage Aqueous Metal-Ion Batteries Beyond 1.5 V: The Zinc/Zinc Hexacyanoferrate System, Adv. Energy Mater., 2015, 5, 1400930.
- 14 G. Kasiri, J. Glenneberg, A. Bani Hashemi, R. Kun and F. La Mantia, Mixed Copper-Zinc Hexacyanoferrates as Cathode Materials for Aqueous Zinc-Ion Batteries, Energy Storage Mater., 2019, 19, 360-369.
- 15 Z. Guo, Y. Ma, X. Dong, J. Huang, Y. Wang and Y. Xia, An Environmentally Friendly and Flexible Aqueous Zinc Battery Using an Organic Cathode, Angew. Chem., Int. Ed., 2018, 57, 11737-11741.
- 16 D. Kundu, P. Oberholzer, C. Glaros, A. Bouzid, E. Tervoort, A. Pasquarello and M. Niederberger, Organic Cathode for Aqueous Zn-Ion Batteries: Taming a Unique Phase Evolution toward Stable Electrochemical Cycling, Chem. Mater., 2018, 30, 3874-3881.
- 17 C. GassnerGalvanic Battery, US Pat., US373064A, 1887.
- 18 T. A. EdisonReversible Galvanic Battery, US Pat., US704304A, 1901.
- 19 S. Raghav; J. Raghav; P. K. Yadav and D. Kumar, Alkaline Batteries, in Rechargeable Batteries, 2020, pp. 357–378.
- 20 L. Binder, W. Odar and K. Kordesch, A Study of Rechargeable Zinc Electrodes for Alkaline Cells Requiring Anodic Limitation, J. Power Sources, 1981, 6, 271–289.
- 21 R. Shivkumar, G. Paruthimal Kalaignan and T. Vasudevan, Effect of Additives on Zinc Electrodes in Alkaline Battery Systems, J. Power Sources, 1995, 55, 53-62.
- 22 G. RampelDendrite-Inhibiting Additive for Battery Cell Having Zinc Electrode, US Pat., US3660170A, 1970.

- 23 T. Shoji, M. Hishinuma and T. Yamamoto, Zinc-Manganese Dioxide Galvanic Cell Using Zinc Sulphate as Electrolyte. Rechargeability of the Cell, J. Appl. Electrochem., 1988, 18, 521-526.
- 24 E. Peled, The Electrochemical Behavior of Alkali and Alkaline Earth Metals in Nonaqueous Battery Systemsthe Solid Electrolyte Interphase Model, J. Electrochem. Soc., 1979, 126, 2047-2051.
- 25 E. Peled and S. Menkin, Review-SEI: Past, Present and Future, J. Electrochem. Soc., 2017, 164, A1703-A1719.
- 26 L. Cao, D. Li, E. Hu, J. Xu, T. Deng, L. Ma, Y. Wang, X.-Q. Yang and C. Wang, Solvation Structure Design for Aqueous Zn Metal Batteries, J. Am. Chem. Soc., 2020, 142, 21404-21409.
- 27 C. Li, R. Kingsbury, L. Zhou, A. Shyamsunder, K. A. Persson and L. F. Nazar, Tuning the Solvation Structure in Aqueous Zinc Batteries to Maximize Zn-Ion Intercalation and Optimize Dendrite-Free Zinc Plating, ACS Energy Lett., 2022, 7, 533-540.
- 28 J. Cao, D. Zhang, X. Zhang, Z. Zeng, J. Qin and Y. Huang, Strategies of Regulating Zn2+ Solvation Structures for Dendrite-Free and Side Reaction-Suppressed Zinc-Ion Batteries, Energy Environ. Sci., 2022, 15, 499-528.
- 29 W. Sun, et al., A Rechargeable Zinc-Air Battery Based on Zinc Peroxide Chemistry, Science, 2021, 371, 46-51.
- 30 L. Ma, et al., Functionalized Phosphonium Cations Enable Zinc Metal Reversibility in Aqueous Electrolytes, Angew. Chem., Int. Ed., 2021, 60, 12438-12445.
- 31 L. Cao, et al., Fluorinated Interphase Enables Reversible Aqueous Zinc Battery Chemistries, Nat. Nanotechnol., 2021, 16, 902-910.
- 32 X. Zeng, et al., Bio-Inspired Design of an in Situ Multifunctional Polymeric Solid-Electrolyte Interphase for Zn Metal Anode Cycling at 30 mA cm<sup>-2</sup> and 30 mAh cm<sup>-2</sup>, Energy Environ. Sci., 2021, **14**, 5947–5957.
- 33 X. He, et al., Anion Concentration Gradient-Assisted Construction of a Solid-Electrolyte Interphase for a Stable Zinc Metal Anode at High Rates, J. Am. Chem. Soc., 2022, 144, 11168-11177.
- 34 M. Liu, L. Yang, H. Liu, A. Amine, Q. Zhao, Y. Song, J. Yang, K. Wang and F. Pan, Artificial Solid-Electrolyte Interface Facilitating Dendrite-Free Zinc Metal Anodes Via Nanowetting Effect, ACS Appl. Mater. Interfaces, 2019, 11, 32046-32051.
- 35 Z. Zhao, J. Zhao, Z. Hu, J. Li, J. Li, Y. Zhang, C. Wang and G. Cui, Long-Life and Deeply Rechargeable Aqueous Zn Anodes Enabled by a Multifunctional Brightener-Inspired Interphase, Energy Environ. Sci., 2019, 12, 1938–1949.
- 36 D. Li, L. Cao, T. Deng, S. Liu and C. Wang, Design of a Solid Electrolyte Interphase for Aqueous Zn Batteries, Angew. Chem., Int. Ed., 2021, 60, 13035-13041.
- 37 L. Ma, Q. Li, Y. Ying, F. Ma, S. Chen, Y. Li, H. Huang and C. Zhi, Toward Practical High-Areal-Capacity Aqueous Zinc-Metal Batteries: Quantifying Hydrogen Evolution and a Solid-Ion Conductor for Stable Zinc Anodes, Adv. Mater., 2021, 33, 2007406.

- 38 J. Han, H. Euchner, M. Kuenzel, S. M. Hosseini, A. Groß, A. Varzi and S. Passerini, A Thin and Uniform Fluoride-Based Artificial Interphase for the Zinc Metal Anode Enabling Reversible Zn/MnO<sub>2</sub> Batteries, ACS Energy Lett., 2021, 6, 3063–3071.
- 39 L. Ma, *et al.*, Highly Reversible Zn Metal Anode Enabled by Sustainable Hydroxyl Chemistry, *Proc. Natl. Acad. Sci.*, 2022, **119**, e2121138119.
- 40 Y. Liu, J. Zhi, T. K. A. Hoang, M. Zhou, M. Han, Y. Wu, Q. Shi, R. Xing and P. Chen, Paraffin Based Cathode– Electrolyte Interface for Highly Reversible Aqueous Zinc-Ion Battery, ACS Appl. Energy Mater., 2022, 5, 4840–4849.
- 41 M. Zhou, Y. Chen, G. Fang and S. Liang, Electrolyte/ Electrode Interfacial Electrochemical Behaviors and Optimization Strategies in Aqueous Zinc-Ion Batteries, *Energy Storage Mater.*, 2022, 45, 618–646.
- 42 S. Guo, S. Liang, B. Zhang, G. Fang, D. Ma and J. Zhou, Cathode Interfacial Layer Formation Via in Situ Electrochemically Charging in Aqueous Zinc-Ion Battery, *ACS Nano*, 2019, **13**, 13456–13464.
- 43 Q. Zhao, X. Huang, M. Zhou, Z. Ju, X. Sun, Y. Sun, Z. Huang, H. Li and T. Ma, Proton Insertion Promoted a Polyfurfural/ MnO<sub>2</sub> Nanocomposite Cathode for a Rechargeable Aqueous Zn-Mno2 Battery, ACS Appl. Mater. Interfaces, 2020, 12, 36072–36081.
- 44 J. Guo, J. Ming, Y. Lei, W. Zhang, C. Xia, Y. Cui and H. N. Alshareef, Artificial Solid Electrolyte Interphase for Suppressing Surface Reactions and Cathode Dissolution in Aqueous Zinc Ion Batteries, ACS Energy Lett., 2019, 4, 2776–2781.
- 45 J. B. Goodenough and Y. Kim, Challenges for Rechargeable Li Batteries, *Chem. Mater.*, 2010, 22, 587–603.
- 46 L. Ma, *et al.*, Ammonium Enables Reversible Aqueous Zn Battery Chemistries by Tailoring the Interphase, *One Earth*, 2022, 5, 413–421.
- 47 L. Ma and C. Zhi, Zn Electrode/Electrolyte Interfaces of Zn Batteries: A Mini Review, *Electrochem. Commun.*, 2021, 122, 106898.
- 48 A. Naveed, A. Ali, T. Rasheed, X. Wang, P. Ye, X. Li, Y. Zhou, S. Mingru and Y. Liu, Revisiting Recent and Traditional Strategies for Surface Protection of Zn Metal Anode, *J. Power Sources*, 2022, 525, 231122.
- 49 S. Guo, L. Qin, T. Zhang, M. Zhou, J. Zhou, G. Fang and S. Liang, Fundamentals and Perspectives of Electrolyte Additives for Aqueous Zinc-Ion Batteries, *Energy Storage Mater.*, 2021, 34, 545–562.
- 50 J. Mink, C. Németh, L. Hajba, M. Sandström and P. L. Goggin, Infrared and Raman Spectroscopic and Theoretical Studies of Hexaaqua Metal Ions in Aqueous Solution, J. Mol. Struct., 2003, 661–662, 141–151.
- 51 J. Hao, L. Yuan, C. Ye, D. Chao, K. Davey, Z. Guo and S.-Z. Qiao, Boosting Zinc Electrode Reversibility in Aqueous Electrolytes by Using Low-Cost Antisolvents, Angew. Chem., Int. Ed., 2021, 60, 7366–7375.
- 52 J. Duan, L. Min, T. Yang, M. Chen and C. Wang, High-Performance and Dendrite-Free Zn/Kznhcf Batteries

- Boosted by Aqueous Electrolyte Mixed with Ethanol, *J. Alloys Compd.*, 2022, **918**, 165619.
- 53 V. Verma, R. M. Chan, L. Jia Yang, S. Kumar, S. Sattayaporn, R. Chua, Y. Cai, P. Kidkhunthod, W. Manalastas and M. Srinivasan, Chelating Ligands as Electrolyte Solvent for Rechargeable Zinc-Ion Batteries, *Chem. Mater.*, 2021, 33, 1330–1340.
- 54 X. Li, H. Wang, X. Sun, J. Li and Y.-N. Liu, Flexible Wide-Temperature Zinc-Ion Battery Enabled by an Ethylene Glycol-Based Organohydrogel Electrolyte, *ACS Appl. Energy Mater.*, 2021, 4, 12718–12727.
- 55 N. Wang, Y. Yang, X. Qiu, X. Dong, Y. Wang and Y. Xia, Stabilized Rechargeable Aqueous Zinc Batteries Using Ethylene Glycol as Water Blocker, *ChemSusChem*, 2020, 13, 5556–5564.
- 56 A. S. Etman, M. Carboni, J. Sun and R. Younesi, Acetonitrile-Based Electrolytes for Rechargeable Zinc Batteries, *Energy Technol.*, 2020, 8, 2000358.
- 57 J. Shi, K. Xia, L. Liu, C. Liu, Q. Zhang, L. Li, X. Zhou, J. Liang and Z. Tao, Ultrahigh Coulombic Efficiency and Long-Life Aqueous Zn Anodes Enabled by Electrolyte Additive of Acetonitrile, *Electrochim. Acta*, 2020, 358, 136937.
- 58 W. Yang, *et al.*, Hydrated Eutectic Electrolytes with Ligand-Oriented Solvation Shells for Long-Cycling Zinc-Organic Batteries, *Joule*, 2020, **4**, 1557–1574.
- 59 B. Kakoty, R. Vengarathody, S. Mukherji, V. Ahuja, A. Joseph, C. Narayana, S. Balasubramanian and P. Senguttuvan, Two for One: Propylene Carbonate Co-Solvent for High Performance Aqueous Zinc-Ion Batterie–Remedies for Persistent Issues at Both Electrodes, *J. Mater. Chem. A*, 2022, 10, 12597–12607.
- 60 F. Ming, Y. Zhu, G. Huang, A.-H. Emwas, H. Liang, Y. Cui and H. N. Alshareef, Co-Solvent Electrolyte Engineering for Stable Anode-Free Zinc Metal Batteries, *J. Am. Chem. Soc.*, 2022, 144, 7160–7170.
- 61 W. Kao-ian, M. T. Nguyen, T. Yonezawa, R. Pornprasertsuk, J. Qin, S. Siwamogsatham and S. Kheawhom, Highly Stable Rechargeable Zinc-Ion Battery Using Dimethyl Sulfoxide Electrolyte, *Mater. Today Energy*, 2021, 21, 100738.
- 62 X. Lin, G. Zhou, M. J. Robson, J. Yu, S. C. T. Kwok and F. Ciucci, Hydrated Deep Eutectic Electrolytes for High-Performance Zn-Ion Batteries Capable of Low-Temperature Operation, *Adv. Funct. Mater.*, 2022, 32, 2109322.
- 63 B. Qiu, L. Xie, G. Zhang, K. Cheng, Z. Lin, W. Liu, C. He, P. Zhang and H. Mi, Toward Reversible Wide-Temperature Zn Storage by Regulating the Electrolyte Solvation Structure Via Trimethyl Phosphate, *Chem. Eng. J.*, 2022, 449, 137843.
- 64 S. Liu, J. Mao, W. K. Pang, J. Vongsvivut, X. Zeng, L. Thomsen, Y. Wang, J. Liu, D. Li and Z. Guo, Tuning the Electrolyte Solvation Structure to Suppress Cathode Dissolution, Water Reactivity, and Zn Dendrite Growth in Zinc-Ion Batteries, Adv. Funct. Mater., 2021, 31, 2104281.
- 65 S. Liu, J. Vongsvivut, Y. Wang, R. Zhang, F. Yang, S. Zhang, K. Davey, J. Mao and Z. Guo, Monolithic Phosphate

- Interphase for Highly Reversible and Stable Zn Metal Anode, Angew. Chem., Int. Ed., 2023, 62, e202215600.
- 66 L. Miao, R. Wang, W. Xin, L. Zhang, Y. Geng, H. Peng, Z. Yan, D. Jiang, Z. Qian and Z. Zhu, Three-Functional Ether-Based Co-Solvents for Suppressing Water-Induced Parasitic Reactions in Aqueous Zn-Ion Batteries, Energy Storage Mater., 2022, 49, 445-453.
- 67 T. Melin, R. Lundström and E. J. Berg, Revisiting the Ethylene Carbonate-Propylene Carbonate Mystery with Operando Characterization, Adv. Mater. Interfaces, 2022, 9, 2101258.
- 68 Q. Qian, Y. Yang and H. Shao, Solid Electrolyte Interphase Formation by Propylene Carbonate Reduction for Lithium Anode, Phys. Chem. Chem. Phys., 2017, 19, 28772-28780.
- 69 D. Xu, Z.-l. Wang, J.-j. Xu, L.-l. Zhang and X.-b. Zhang, Novel Dmso-Based Electrolyte for High Performance Rechargeable Li-O<sub>2</sub> Batteries, Chem. Commun., 2012, 48, 6948-6950.
- 70 O. Borodin, Challenges with Prediction of Battery Electrolyte Electrochemical Stability Window and Guiding Electrode-Electrolyte Stabilization, Electrochem., 2019, 13, 86-93.
- 71 A. Naveed, H. Yang, J. Yang, Y. Nuli and J. Wang, Highly Reversible and Rechargeable Safe Zn Batteries Based on a Triethyl Phosphate Electrolyte, Angew. Chem., Int. Ed., 2019, 58, 2760-2764.
- 72 A. Naveed, et al., A Highly Reversible Zn Anode with Intrinsically Safe Organic Electrolyte for Long-Cycle-Life Batteries, Adv. Mater., 2019, 31, 1900668.
- 73 L. Ma, M. A. Schroeder, O. Borodin, T. P. Pollard, M. S. Ding, C. Wang and K. Xu, Realizing High Zinc Reversibility in Rechargeable Batteries, Nat. Energy, 2020, 5, 743-749.
- 74 F. Wang, O. Borodin, T. Gao, X. Fan, W. Sun, F. Han, A. Faraone, J. A. Dura, K. Xu and C. Wang, Highly Reversible Zinc Metal Anode for Aqueous Batteries, Nat. Mater., 2018, 17, 543-549.
- 75 H. Yan, S. Li, H. Xu, H. Chen, S. Yang and B. Li, Triggering Zn<sup>2+</sup> Unsaturated Hydration Structure Via Hydrated Salt Electrolyte for High Voltage and Cycling Stable Rechargeable Aqueous Zn Battery, Adv. Energy Mater., 2022, 12, 2201599.
- 76 L. Wang, Y. Zhang, H. Hu, H.-Y. Shi, Y. Song, D. Guo, X.-X. Liu and X. Sun, A Zn(ClO<sub>4</sub>)<sub>2</sub> Electrolyte Enabling Long-Life Zinc Metal Electrodes for Rechargeable Aqueous Zinc Batteries, ACS Appl. Mater. Interfaces, 2019, 11, 42000-42005.
- 77 X. Zeng, J. Liu, J. Mao, J. Hao, Z. Wang, S. Zhou, C. D. Ling and Z. Guo, Toward a Reversible Mn<sup>4+</sup>/Mn<sup>2+</sup> Redox Reaction and Dendrite-Free Zn Anode in near-Neutral Aqueous Zn/Mno2 Batteries Via Salt Anion Chemistry, Adv. Energy Mater., 2020, 10, 1904163.
- 78 L. Suo, O. Borodin, T. Gao, M. Olguin, J. Ho, X. Fan, C. Luo, C. Wang and K. Xu, Electrolyte Enables High-Voltage Aqueous Lithium-Ion Chemistries, Science, 2015, 350, 938-943.

- 79 Q. Zhang, Y. Ma, Y. Lu, L. Li, F. Wan, K. Zhang and J. Chen, Modulating Electrolyte Structure for Ultralow Temperature Aqueous Zinc Batteries, Nat. Commun., 2020, 11, 4463.
- 80 C. Zhang, et al., A Zncl2 Water-in-Salt Electrolyte for a Reversible Zn Metal Anode, Chem. Commun., 2018, 54, 14097-14099.
- 81 L. Zhang, I. A. Rodríguez-Pérez, H. Jiang, C. Zhang, D. P. Leonard, Q. Guo, W. Wang, S. Han, L. Wang and X. Ji, ZnCl<sub>2</sub> "Water-in-Salt" Electrolyte Transforms the Performance of Vanadium Oxide as a Zn Battery Cathode, Adv. Funct. Mater., 2019, 29, 1902653.
- 82 S. Chen, R. Lan, J. Humphreys and S. Tao, Salt-Concentrated Acetate Electrolytes for a High Voltage Aqueous Zn/Mno2 Battery, Energy Storage Mater., 2020, 28, 205-215.
- 83 S. Chen, P. Sun, J. Humphreys, P. Zou, M. Zhang, G. Jeerh, B. Sun and S. N. Tao, N-Dimethylacetamide-Diluted Nitrate Electrolyte for Aqueous Zn//LiMn<sub>2</sub>O<sub>4</sub> Hybrid Ion Batteries, ACS Appl. Mater. Interfaces, 2021, 13, 46634-46643.
- 84 H. Glatz, E. Tervoort and D. Kundu, Unveiling Critical Insight into the Zn Metal Anode Cyclability in Mildly Acidic Aqueous Electrolytes: Implications for Aqueous Zinc Batteries, ACS Appl. Mater. Interfaces, 2020, 12, 3522-3530.
- 85 L. Ma, et al., Critical Factors Dictating Reversibility of the Zinc Metal Anode, Energy Environ. Mater., 2020, 3, 516-521.
- 86 Z. A. Zafar, G. Abbas, K. Knizek, M. Silhavik, P. Kumar, P. Jiricek, J. Houdková, O. Frank and J. Cervenka, Chaotropic Anion Based "Water-in-Salt" Electrolyte Realizes a High Voltage Zn-Graphite Dual-Ion Battery, J. Mater. Chem. A, 2022, 10, 2064-2074.
- 87 F. Wang, W. Sun, Z. Shadike, E. Hu, X. Ji, T. Gao, X.-Q. Yang, K. Xu and C. Wang, How Water Accelerates Bivalent Ion Diffusion at the Electrolyte/Electrode Interface, Angew. Chem., Int. Ed., 2018, 57, 11978-11981.
- 88 S. Chen, R. Lan, J. Humphreys and S. Tao, Perchlorate Based "Oversaturated Gel Electrolyte" for an Aqueous Rechargeable Hybrid Zn-Li Battery, ACS Appl. Energy Mater., 2020, 3, 2526-2536.
- 89 K. Xu, Electrolytes and Interphases in Li-Ion Batteries and Beyond, Chem. Rev., 2014, 114, 11503-11618.
- 90 X. Zeng, et al., Electrolyte Design for in Situ Construction of Highly Zn<sup>2+</sup>-Conductive Solid Electrolyte Interphase to Enable High-Performance Aqueous Zn-Ion Batteries under Practical Conditions, Adv. Mater., 2021, 33, 2007416.
- 91 A. Bayaguud, X. Luo, Y. Fu and C. Zhu, Cationic Surfactant-Type Electrolyte Additive Enables Three-Dimensional Dendrite-Free Zinc Anode for Stable Zinc-Ion Batteries, ACS Energy Lett., 2020, 5, 3012-3020.
- 92 S.-J. Zhang, J. Hao, D. Luo, P.-F. Zhang, B. Zhang, K. Davey, Z. Lin and S.-Z. Qiao, Dual-Function Electrolyte Additive for Highly Reversible Zn Anode, Adv. Energy Mater., 2021, 11, 2102010.
- 93 K. Xie, K. Ren, C. Sun, S. Yang, M. Tong, S. Yang, Z. Liu and O. Wang, Toward Stable Zinc-Ion Batteries: Use of a Chelate Electrolyte Additive for Uniform Zinc Deposition, ACS Appl. Energy Mater., 2022, 5, 4170-4178.

- 94 K. Zhao, F. Liu, G. Fan, J. Liu, M. Yu, Z. Yan, N. Zhang and F. Cheng, Stabilizing Zinc Electrodes with a Vanillin Additive in Mild Aqueous Electrolytes, *ACS Appl. Mater. Interfaces*, 2021, 13, 47650–47658.
- 95 P. Sun, L. Ma, W. Zhou, M. Qiu, Z. Wang, D. Chao and W. Mai, Simultaneous Regulation on Solvation Shell and Electrode Interface for Dendrite-Free Zn Ion Batteries Achieved by a Low-Cost Glucose Additive, *Angew. Chem., Int. Ed.*, 2021, **60**, 18247–18255.
- 96 X. Guo, et al., Alleviation of Dendrite Formation on Zinc Anodes Via Electrolyte Additives, ACS Energy Lett., 2021, 6, 395–403.
- 97 Y. Jin, K. S. Han, Y. Shao, M. L. Sushko, J. Xiao, H. Pan and J. Liu, Stabilizing Zinc Anode Reactions by Polyethylene Oxide Polymer in Mild Aqueous Electrolytes, *Adv. Funct. Mater.*, 2020, **30**, 2003932.
- 98 M. Yan, C. Xu, Y. Sun, H. Pan and H. Li, Manipulating Zn Anode Reactions through Salt Anion Involving Hydrogen Bonding Network in Aqueous Electrolytes with Peo Additive, *Nano Energy*, 2021, **82**, 105739.
- 99 W. Deng, Z. Xu and X. Wang, High-Donor Electrolyte Additive Enabling Stable Aqueous Zinc-Ion Batteries, *Energy Storage Mater.*, 2022, **52**, 52–60.
- 100 R. Zhao, H. Wang, H. Du, Y. Yang, Z. Gao, L. Qie and Y. Huang, Lanthanum Nitrate as Aqueous Electrolyte Additive for Favourable Zinc Metal Electrodeposition, *Nat. Commun.*, 2022, 13, 3252.
- 101 Z. Jia, W. Zhao, S. Hu, X. Yang, T. He and X. Sun, An Amphoteric Betaine Electrolyte Additive Enabling a Stable Zn Metal Anode for Aqueous Batteries, *Chem. Commun.*, 2022, 58, 8504–8507.
- 102 C. Lin, X. Yang, P. Xiong, H. Lin, L. He, Q. Yao, M. Wei, Q. Qian, Q. Chen and L. Zeng, High-Rate, Large Capacity, and Long Life Dendrite-Free Zn Metal Anode Enabled by Trifunctional Electrolyte Additive with a Wide Temperature Range, Adv. Sci., 2022, 9, 2201433.
- 103 K. Guan, L. Tao, R. Yang, H. Zhang, N. Wang, H. Wan, J. Cui, J. Zhang, H. Wang and H. Wang, Anti-Corrosion for Reversible Zinc Anode Via a Hydrophobic Interface in Aqueous Zinc Batteries, Adv. Energy Mater., 2022, 12, 2103557.
- 104 S. Di, X. Nie, G. Ma, W. Yuan, Y. Wang, Y. Liu, S. Shen and N. Zhang, Zinc Anode Stabilized by an Organic-Inorganic Hybrid Solid Electrolyte Interphase, *Energy Storage Mater.*, 2021, 43, 375–382.
- 105 Z. Li, et al., Uniformizing the Electric Field Distribution and Ion Migration During Zinc Plating/Stripping Via a Binary Polymer Blend Artificial Interphase, J. Mater. Chem. A, 2020, 8, 17725–17731.
- 106 J. Hao, X. Li, S. Zhang, F. Yang, X. Zeng, S. Zhang, G. Bo, C. Wang and Z. Guo, Designing Dendrite-Free Zinc Anodes for Advanced Aqueous Zinc Batteries, *Adv. Funct. Mater.*, 2020, 30, 2001263.
- 107 Y. Yang, *et al.*, Redistributing Zn-Ion Flux by Interlayer Ion Channels in Mg-Al Layered Double Hydroxide-Based Artificial Solid Electrolyte Interface for Ultra-Stable and

- Dendrite-Free Zn Metal Anodes, *Energy Storage Mater.*, 2021, 41, 230–239.
- 108 H. Peng, Y. Fang, J. Wang, P. Ruan, Y. Tang, B. Lu, X. Cao, S. Liang and J. Zhou, Constructing Fast-Ion-Conductive Disordered Interphase for High-Performance Zinc-Ion and Zinc-Iodine Batteries, *Matter*, 2022, 5, 4363–4378.
- 109 W. Zhang, Q. Zhao, Y. Hou, Z. Shen, L. Fan, S. Zhou, Y. Lu and L. A. Archer, Dynamic Interphase—Mediated Assembly for Deep Cycling Metal Batteries, *Sci. Adv.*, 2021, 7, eabl3752.
- 110 Y. Wang, Y. Liu, H. Wang, S. Dou, W. Gan, L. Ci, Y. Huang and Q. Yuan, MOF-Based Ionic Sieve Interphase for Regulated Zn<sup>2+</sup> Flux toward Dendrite-Free Aqueous Zinc-Ion Batteries, *J. Mater. Chem. A*, 2022, **10**, 4366–4375.
- 111 L. Cao, D. Li, T. Deng, Q. Li and C. Wang, Hydrophobic Organic-Electrolyte-Protected Zinc Anodes for Aqueous Zinc Batteries, *Angew. Chem., Int. Ed.*, 2020, **59**, 19292–19296.
- 112 L. Godeffroy, I. Aguilar, J. Médard, D. Larcher, J.-M. Tarascon and F. Kanoufi, Decoupling the Dynamics of Zinc Hydroxide Sulfate Precipitation/Dissolution in Aqueous Zn-MnO<sub>2</sub> Batteries by Operando Optical Microscopy: A Missing Piece of the Mechanistic Puzzle, Adv. Energy Mater., 2022, 12, 2200722.
- 113 B. Lee, H. R. Seo, H. R. Lee, C. S. Yoon, J. H. Kim, K. Y. Chung, B. W. Cho and S. H. Oh, Critical Role of Ph Evolution of Electrolyte in the Reaction Mechanism for Rechargeable Zinc Batteries, *ChemSusChem*, 2016, 9, 2948–2956.
- 114 I. A. Rodríguez-Pérez, H. J. Chang, M. Fayette, B. M. Sivakumar, D. Choi, X. Li and D. Reed, Mechanistic Investigation of Redox Processes in Zn–Mno2 Battery in Mild Aqueous Electrolytes, *J. Mater. Chem. A*, 2021, 9, 20766–20775.
- 115 O. Fitz, C. Bischoff, M. Bauer, H. Gentischer, K. P. Birke, H.-M. Henning and D. Biro, Electrolyte Study with in Operando Ph Tracking Providing Insight into the Reaction Mechanism of Aqueous Acidic Zn//MnO<sub>2</sub> Batteries, *ChemElectroChem*, 2021, 8, 3553–3566.
- 116 P. Oberholzer, E. Tervoort, A. Bouzid, A. Pasquarello and D. Kundu, Oxide Versus Nonoxide Cathode Materials for Aqueous Zn Batteries: An Insight into the Charge Storage Mechanism and Consequences Thereof, ACS Appl. Mater. Interfaces, 2019, 11, 674–682.
- 117 M. H. Alfaruqi, S. Islam, D. Y. Putro, V. Mathew, S. Kim, J. Jo, S. Kim, Y.-K. Sun, K. Kim and J. Kim, Structural Transformation and Electrochemical Study of Layered MnO<sub>2</sub> in Rechargeable Aqueous Zinc-Ion Battery, *Electrochim. Acta*, 2018, 276, 1–11.
- 118 B. Lee, C. S. Yoon, H. R. Lee, K. Y. Chung, B. W. Cho and S. H. Oh, Electrochemically-Induced Reversible Transition from the Tunneled to Layered Polymorphs of Manganese Dioxide, *Sci. Rep.*, 2014, 4, 6066.
- 119 Z. Hou, M. Dong, Y. Xiong, X. Zhang, H. Ao, M. Liu, Y. Zhu and Y. Qian, A High-Energy and Long-Life Aqueous Zn/Birnessite Battery Via Reversible Water and Zn<sup>2+</sup> Coinsertion, *Small*, 2020, **16**, 2001228.

- 120 L. Zhang, B. Zhang, J. Hu, J. Liu, L. Miao and J. Jiang, An in Situ Artificial Cathode Electrolyte Interphase Strategy for Suppressing Cathode Dissolution in Aqueous Zinc Ion Batteries, Small Methods, 2021, 5, 2100094.
- 121 M. Han, J. Zhi, T. K. A. Hoang, Y. Li, L. Li and P. Chen, Artificial Solid Electrolyte Interphase for Thermally Stable Rechargeable Aqueous Zinc Batteries, J. Power Sources, 2019, 441, 227171.
- 122 Z. Tie and Z. Niu, Design Strategies for High-Performance Aqueous Zn/Organic Batteries, Angew. Chem., Int. Ed., 2020, 59, 21293-21303.
- 123 J. Hao, B. Li, X. Li, X. Zeng, S. Zhang, F. Yang, S. Liu, D. Li, C. Wu and Z. Guo, An in-Depth Study of Zn Metal Surface Chemistry for Advanced Aqueous Zn-Ion Batteries, Adv. Mater., 2020, 32, 2003021.
- 124 W. Shin, J. Lee, Y. Kim, H. Steinfink and A. Heller, Ionic Conduction in Zn<sub>3</sub>(PO<sub>4</sub>)<sub>2</sub>·4H<sub>2</sub>O Enables Discharge of the Zinc Anode in Serum, J. Am. Chem. Soc., 2005, 127, 14590-14591.
- 125 W. Xin, L. Miao, L. Zhang, H. Peng, Z. Yan and Z. Zhu, Turning the Byproduct Zn<sub>4</sub>(OH)<sub>6</sub>SO<sub>4</sub>·xH<sub>2</sub>O into a Uniform Solid Electrolyte Interphase to Stabilize Aqueous Zn Anode, ACS Mater. Lett., 2021, 3, 1819-1825.
- 126 J. Shin, J. Lee, Y. Kim, Y. Park, M. Kim and J. W. Choi, Highly Reversible, Grain-Directed Zinc Deposition in Aqueous Zinc Ion Batteries, Adv. Energy Mater., 2021, 11, 2100676.
- 127 X. Cao, et al., Monolithic Solid-Electrolyte Interphases Formed in Fluorinated Orthoformate-Based Electrolytes Minimize Li Depletion and Pulverization, Nat. Energy, 2019, 4, 796-805.
- 128 M. Nie, J. Demeaux, B. T. Young, D. R. Heskett, Y. Chen, A. Bose, J. C. Woicik and B. L. Lucht, Effect of Vinylene Carbonate and Fluoroethylene Carbonate on SEI Formation on Graphitic Anodes in Li-Ion Batteries, I. Electrochem. Soc., 2015, 162, A7008-A7014.
- 129 C. Yuan, W. Lu and J. Xu, Unlocking the Electrochemical-Mechanical Coupling Behaviors of Dendrite Growth and Crack Propagation in All-Solid-State Batteries, Adv. Energy Mater., 2021, 11, 2101807.
- 130 Q. Yang, Q. Li, Z. Liu, D. Wang, Y. Guo, X. Li, Y. Tang, H. Li, B. Dong and C. Zhi, Dendrites in Zn-Based Batteries, Adv. Mater., 2020, 32, 2001854.
- 131 Z. Li, L. Wu, S. Dong, T. Xu, S. Li, Y. An, J. Jiang and X. Zhang, Pencil Drawing Stable Interface for Reversible and Durable Aqueous Zinc-Ion Batteries, Adv. Funct. Mater., 2021, 31, 2006495.

- 132 P. Sun, W. Liu, D. Yang, Y. Zhang, W. Xiong, S. Li, J. Chen, J. Tian and L. Zhang, Stable Zn Anodes Enabled by High-Modulus Agarose Gel Electrolyte with Confined Water Molecule Mobility, Electrochim. Acta, 2022, 429, 140985.
- 133 Z. Ahmad, T. Xie, C. Maheshwari, J. C. Grossman and v. Machine Learning Viswanathan, **Enabled** Computational Screening of Inorganic Solid Electrolytes for Suppression of Dendrite Formation in Lithium Metal Anodes, ACS Cent. Sci., 2018, 4, 996-1006.
- 134 N. N. Sinha, A. J. Smith, J. C. Burns, G. Jain, K. W. Eberman, E. Scott, J. P. Gardner and J. R. Dahn, The Use of Elevated Temperature Storage Experiments to Learn About Parasitic Reactions in Wound LiCoO2/Graphite Cells, J. Electrochem. Soc., 2011, 158, A1194.
- 135 A. J. Smith, J. C. Burns and J. R. Dahn, A High Precision Study of the Coulombic Efficiency of Li-Ion Batteries, Electrochem. Solid-State Lett., 2010, 13, A177.
- 136 L. Suo, et al., How Solid-Electrolyte Interphase Forms in Aqueous Electrolytes, J. Am. Chem. Soc., 2017, 139, 18670-18680.
- Li<sup>+</sup> 137 B. Nan, et al., Enhancing Transport NMC811||Graphite Lithium-Ion **Batteries** Low Temperatures by Using Low-Polarity-Solvent Electrolytes, Angew. Chem., Int. Ed., 2022, 61, e202205967.
- 138 K. Y. Kwon, S. J. Kim, D.-M. Kim, H. Kim, S. K. Mohanty, K. T. Lee and H. D. Yoo, Potential-Dependent Passivation of Zinc Metal in a Sulfate-Based Aqueous Electrolyte, Langmuir, 2021, 37, 13218-13224.
- 139 X. Zhou, Y. Lu, Q. Zhang, L. Miao, K. Zhang, Z. Yan, F. Li and J. Chen, Exploring the Interfacial Chemistry between Zinc Anodes and Aqueous Electrolytes Via an in Situ Visualized Characterization System, ACS Appl. Mater. Interfaces, 2020, 12, 55476-55482.
- 140 G. Feng, et al., Imaging Solid-Electrolyte Interphase Dynamics Using Operando Reflection Interference Microscopy, Nat. Nanotechnol., 2023, DOI: 10.1038/s41565-023-01316-3.
- 141 A. J. Smith, J. C. Burns, X. Zhao, D. Xiong and J. R. Dahn, A High Precision Coulometry Study of the Sei Growth in Li/ Graphite Cells, J. Electrochem. Soc., 2011, 158, A447.
- 142 H. J. Ploehn, P. Ramadass and R. E. White, Solvent Diffusion Model for Aging of Lithium-Ion Battery Cells, J. Electrochem. Soc., 2004, 151, A456.
- 143 J. C. Burns, G. Jain, A. J. Smith, K. W. Eberman, E. Scott, J. P. Gardner and J. R. Dahn, Evaluation of Effects of Additives in Wound Li-Ion Cells through High Precision Coulometry, J. Electrochem. Soc., 2011, 158, A255.